A Generalized Overmodulation Strategy With Minimum Current Distortion for Symmetrical and Asymmetrical Multiphase Induction Motor Drives

Martín Medina-Sánchez, *Graduate Student Member, IEEE*, Alejandro G. Yepes, *Senior Member, IEEE*, Óscar López, *Senior Member, IEEE*, and Jesús Doval-Gandoy, *Member, IEEE*

***Abstract*—Multiphase machines are a promising alternative for high-reliability applications. In these applications, overmodulation (OVM) is important since it allows attaining higher modulation indices by injecting, besides zero-sequence voltage harmonics, current-producing ones. In general, the existing techniques are able to limit to some extent the current total harmonic distortion (THD). However, most do not ensure the minimum current THD, thereby not guaranteeing the minimum harmonic stator copper loss. Furthermore, most are intended just for particular phase numbers n, symmetrical/asymmetrical winding arrangements and neutral-point (NP) configurations. OVM with low THD remains unaddressed in most types of multiphase motors. This article overcomes these limitations by proposing a generalized OVM strategy that attains the minimum current THD in induction motors with any n, winding arrangement, and NP configurations. Two techniques are outlined. One of them injects only non-torque-related harmonics, while the other technique exploits torque-producing harmonics to further reduce the current THD and to attain modulation indices up to square waveform. The superiority of the proposal in terms of current THD is substantiated through studies for multiple kinds of multiphase machines. The experiments are performed by using two six-phase induction motors with symmetrical/asymmetrical windings when 1 and 2 NPs are set.**

***Index Terms*—DC-link utilization, minimum harmonic distortion, multiphase drives, overmodulation (OVM), pulsewidth modulation (PWM).**

I. Introduction

MULTIPHASE machines offer significant advantages over three-phase ones, such as enhanced fault tolerance, lower torque pulsations, and reduced current ratings per phase [1].

Manuscript received 1 October 2023; revised 24 January 2024; accepted 11 March 2024. Date of publication 19 March 2024; date of current version 19 April 2024. This work was supported in part by the Government of Galicia under Grant ED431F 2020/07 and Grant GPC-ED431B 2023/12, in part by the Ministry of Science, Innovation and Universities under the Ramón y Cajal Grant RYC2018-024407-I, and in part by the Spanish State Research Agency (AEI) under project PID2022-136908OBI00/MCIN/AEI/10.13039/501100011033/FEDER-UE. Recommended for publication by Associate Editor T. Shi. *(Corresponding author: Jesús Doval-Gandoy.)*

The authors are with the Applied Power Electronics Technology (APET) Research Group, CINTECX, Universidade de Vigo, 36310 Vigo, Spain (e-mail: martindamian.medina@uvigo.es; agyepes@uvigo.es; olopez@uvigo.es; jdoval@uvigo.es).

This article has supplementary material provided by the authors and color versions of one or more figures available at https://doi.org/10.1109/TPEL.2024.3377677.

Digital Object Identifier 10.1109/TPEL.2024.3377677

TABLE I
Main Features of the Existing Literature and the Proposal

References	n	SWA	AWA	NPs	Minimum current THD
[10], [15]	Any	✓	✓	Any	✗
[6], [11], [17], [14], [18], [19]	5	✓	✗	1	✗
[16]	5	✓	✗	1	✓
[13], [21]	≥ 5 (odd)	✓	✗	1	✗
[12]	≥ 7 (odd)	✓	✗	1	✗
[5], [24], [25]	6	✗	✓	2	✗
Proposal	Any	✓	✓	Any	✓

For these reasons, they are used in leading-edge applications, [2], [3], e.g., in electric automotive vehicles, where it is highly desirable to increase the dc-link utilization [4]. It allows for several performance improvements, such as a wider speed range for a given dc-link voltage [4], [5], or lower dc-link voltage, which reduces the electromagnetic noise [6].

Motors with n phases ($n > 3$) permit exploiting the dc-link voltage in multiple ways thanks to their extra degrees of freedom, which can be mapped into subspaces by using the vector space decomposition [1], [7]. In machines with sinusoidal winding distribution, either with symmetrical winding arrangement (SWA) or asymmetrical winding arrangement (AWA), only the $\alpha\beta_1$ plane produces torque [2]. The remaining subspaces ($\alpha\beta_\sigma$ with $\sigma \neq 1$) are xy planes, or homopolar axes [1]. They typically present a small impedance [1], and may allow current depending on the neutral configuration [7]. In particular, star-connected windings with one or several isolated neutral points (NPs), without zero-sequence (ZS) path to the converter, are usually adopted [1], [8]. To increase to some extent the maximum modulation index in the linear region of pulsewidth modulation (PWM), noncurrent-producing voltage is injected [9]. To this end, one (for a single NP) or multiple (for multiple NPs) min–max ZS injection is often employed [10]. When the voltage reference surpasses the linear region and enters overmodulation (OVM), besides the ZS injection, low-order current-producing harmonics must also be added [5], [11].

There are several OVM approaches, as summarized in Table I. Most of them rely on injecting xy harmonics, without adding $\alpha\beta_1$ ones, which yield torque ripple [11], [12], [13]. Initial attempts were performed for five-phase drives by using only

the two largest $\alpha\beta_1$ space vectors that are the nearest to the voltage reference [14]. It was extended to higher n in [10] and [15]. In any case, it leads to considerable xy currents (current distortion) [13] that may compromise the drive integrity [6]. Notable efforts have been done to mitigate these currents. Passive filters have been suggested in [10] to increase the xy impedance, but they raise the size and cost. Alternatives to decrease the xy currents without filters are discussed next.

Much attention has been devoted to OVM for five-phase machines [6], [11], [16], [17], [18], [19]. In [6], only xy harmonics are injected when the stator copper loss of the machine is below its rated value; otherwise, the injection of $\alpha\beta_1$ harmonics is favored over xy ones to maintain the current distortion within safe values. The main disadvantage of [6] is that, besides being only for five-phase motors, the xy voltage is not optimal, so large currents arise [16]. On the other hand, the methods that minimize the total harmonic distortion (THD), either the voltage THD [11], [17], [18] or the current THD [16], are effective in decreasing the current distortion. The former inject at each sample the minimum xy voltage while avoiding $\alpha\beta_1$ harmonics [11], [17], [18]. They mitigate the current THD but do not ensure its minimum value, which would be required to minimize the harmonic stator copper losses [16], [20]. This limitation was recently overcome by the methods from [16] (for $n = 5$) because they attain the minimum current THD, i.e., the minimum current distortion (MCD). One of the MCD techniques minimizes the current THD by adding just xy voltage. The other MCD approach further diminishes the xy voltage by injecting $\alpha\beta_1$ harmonics to decrease even more the current THD and to fully exploit the dc-link voltage up to the square waveform. However, the offline optimization in [16] is cumbersome because it involves a significant number of variables and constraints. Moreover, the need for the discrete Fourier transform during the optimization also contributes to its complexity. Most importantly, these approaches [11], [16], [17], [18] lack generality, and thus, they are unsuitable for drives with phase numbers other than five.

For SWAs and odd n, only a few methods [12], [13], [21], [22], [23] reduce to some extent the current THD while injecting only xy harmonics. The techniques in [12] and [22], suitable for odd $n \geq 7$, rely on a sequential optimization scheme. The method in [12] adds only low-order harmonics for modulation indices at the beginning of the OVM range, whereas the approach in [22] injects first high-order harmonics. Among them, the strategy in [12] yields less current THD. The method in [13], for $n \geq 5$, establishes a rule of thumb to compute the dwell times of the space vectors to mitigate the current THD. In any case, the techniques in [12], [13], and [22] fail to guarantee the minimum voltage or current THD. The approach [21], for $n \geq 5$, reaches the minimum voltage THD. A particularization of this technique for $n = 9$ is presented in [23]. The method in [21] yields less current THD than those from [12], [13], and [22], at least when one NP is set, but its degree of closeness to the minimum current THD is unclear. On the other hand, OVM with low THD for SWAs with any even n has not been addressed yet.

For AWAs, the OVM techniques with reduced THD are scarce: just $n = 6$ with two NPs was studied in [5], [24], and [25]. Among them, the method in [5] is highlighted since it yields the lowest current THD [25] while covering the entire OVM range available by injecting just xy harmonics. The technique [5] reaches the minimum voltage THD, but it is not clear if it can reach the minimum possible current THD.

In general, previous OVM techniques with a low THD, besides being restricted to particular n and to SWA/AWA, are limited to specific NP configurations (see Table I). For example, the methods from [12], [13], and [21] (for SWAs and odd n) are intended only for one NP, but motors with nonprime n can have several NPs, one per winding set. Similarly, [5], [24], and [25] (just for AWA and $n = 6$) consider only the case when two NPs are set, but one NP provides enhanced fault tolerance [8]. In this regard, addressing OVM for AWA and one NP is challenging since several subspaces become coupled [7], yielding imbalance in phase voltages [26].

As shown in Table I, there is no OVM strategy able to mitigate the current THD for multiphase induction motor drives with any phase number n, winding arrangement, and NPs. Although there are a few techniques that reduce the THD for odd $n > 5$, none of them ensure the MCD. Moreover, the performance of certain existing methods when considering a single or multiple NPs (if applicable) remains unclear.

This article surpasses these limitations by proposing a generalized OVM strategy that attains the minimum current THD, i.e., the MCD, for multiphase induction motor drives with any n and NP configuration, and either SWA or AWA. To achieve the MCD, the proposal injects optimum pole-voltage harmonics that minimize the current THD. To this end, the amplitudes and initial phase angles of these voltage harmonics are found offline, and then, stored in lookup tables, as a function of the modulation index, for commissioning. This optimization is simpler than that in [16] (only for $n = 5$), although its most important contribution is its generality. For several types of multiphase motors, the performance of the most notable existing OVM methods is compared with that of the proposal in terms of current THD. The proposal achieves the smallest current THD in all scenarios. In fact, for most types of multiphase machines considered, this is the first time that OVM with low THD is achieved; e.g., for $n = 6, 12$ with AWA and a single NP, or with SWA and any NPs. The theory is experimentally verified by using two six-phase motors, with either SWA/AWA, when one and two NPs are set.

The rest of this article is organized as follows. Section II describes some essential background. The relationship between the amplitudes of pole- and phase-voltage harmonics is discussed in Section III. The proposal is introduced in Section IV. In Section V, a comprehensive assessment in terms of current THD is addressed. The experimental results are discussed in Section VI, while Section VII concludes this article.

II. Background

A. Vector Space Decomposition and Harmonic Mapping

1) Vector Space Decomposition: There are two main types of winding arrangements in n-phase motors [1]: SWA and AWA. In SWAs, two consecutive stator phases are spatially shifted by

TABLE II
μ SUBSPACES FOR SWA AND AWA WITH 1 OR n/l NPS

	1 NP	n/l NPs
μ subspaces	$\sigma > 1$	$\sigma > 1$, where $\sigma \neq \sigma'$

$\sigma' = \sigma/l \in \mathbb{N}$.

$2\pi/n$. If n is not a prime number, an SWA can be assumed to be comprised of n/l winding sets (ignoring NP connections), with l phases each one, and a spatial displacement of $2\pi/n$ between consecutive sets. Similarly, AWAs also have n/l winding sets with l phases, but with a spatial displacement of π/n between consecutive sets. To facilitate the analysis, their per-phase variable vector

$$\boldsymbol{u} = \begin{bmatrix} u_{\mathrm{a}} & u_{\mathrm{b}} & u_{\mathrm{c}} & \cdots & u_n \end{bmatrix}^{\mathrm{T}} \tag{1}$$

with u being voltage or current, can be mapped into subspaces by means of the vector space decomposition matrix $\boldsymbol{T}$ [1], given in the Appendix. For SWA [7], these subspaces are $\sigma = 0, 1, 2, \ldots, m$, where $m = \lfloor n/2 \rfloor$. All of them are planes, except $\sigma = 0$ and $\sigma = n/2$ for even n, or just $\sigma = 0$ for odd n, which are homopolar axes. On the other hand, for AWA [7], the subspaces are $\sigma = 1, 3, \ldots, m$, where $m = 2\lceil n/2 \rceil - 1$. σ is always a plane, except for odd n, for which $\sigma = n$ is an axis. In general, $\boldsymbol{u}$ is mapped into subspaces, as

$$\begin{bmatrix} \boldsymbol{u_{\alpha\beta,0}} & \boldsymbol{u_{\alpha\beta,1}} & \cdots & \boldsymbol{u_{\alpha\beta,\sigma}} & \cdots & \boldsymbol{u_{\alpha\beta,m}} \end{bmatrix}^{\mathrm{T}} = \boldsymbol{T}\boldsymbol{u} \tag{2}$$

where $\boldsymbol{u_{\alpha\beta,\sigma}}$ is the space vector in the σth subspace $\alpha\beta_\sigma$. For $\alpha\beta_\sigma$ being a plane, $\boldsymbol{u_{\alpha\beta,\sigma}} = u_{\alpha,\sigma} + \mathrm{j}u_{\beta,\sigma}$, where $u_{\alpha,\sigma}$ and $u_{\beta,\sigma}$ are the components along the α_σ and β_σ axes, respectively. Whenever $\alpha\beta_\sigma$ is an axis, $u_{\beta,\sigma} = 0$ and $\boldsymbol{u_{\alpha\beta,\sigma}} = u_{\alpha,\sigma}$. Note that the appropriate σ values for SWA or AWA must be substituted in (2).

The torque is produced only by the $\alpha\beta_1$ plane in machines with nearly sinusoidal winding distribution [1]. The remaining subspaces may allow current depending on the winding arrangement and NPs [5], [7]. For SWA and one NP, there is no current for $\sigma = 0$; for n/l NPs, no current flows for the $\sigma/l \in \mathbb{N}$ subspaces. These $\sigma/l \in \mathbb{N}$ subspaces are denoted as σ'. For AWA and one NP, the σ' subspaces are coupled to each other due to the current constraints, while for n/l NPs, the current is zero for any σ' [7]. In any of these cases, the nontorque subspaces that allow current are termed μ subspaces. They are summarized in Table II.

The notation $Xn\mathrm{N}p$ is used, where $X = \mathrm{S}$ ($X = \mathrm{A}$) stands for SWA (AWA) and p is the number of NPs. For instance, a motor with $n = 6$, AWA and one NP is denoted by A6N1.

2) Voltage Harmonic Mapping: In a voltage-fed motor, the balanced pole-voltage harmonics of order q produced by the inverter are mapped into the σ subspaces as [7]

$$q = \sigma \pm \lambda n \tag{3}$$

where $\lambda = 0, 1, 2\ldots$ for SWA or $\lambda = 0, 2, 4\ldots$ for AWA. The q sign denotes the sequence, where a positive (negative) sign means that the space-vector voltage harmonic rotates, in its corresponding subspace, in the same (opposite) direction as that of the fundamental space-vector voltage. Even values of q are disregarded. For an axis σ, each pole-voltage harmonic in it has both sequences simultaneously $\pm|q|$. In general, the pole-voltage harmonics eventually produce phase-voltage ones. The mapping of the latter is as in (3), except for AWA with one NP, where each pole-voltage harmonic in $\sigma = \sigma'$ yields a phase-voltage counterpart of order $\pm|q|$ [7]. Furthermore, these phase voltages of AWA with one NP exist not only in $\sigma = \sigma'$ but also for every other σ' because of the coupling [7], [26].

As an example, $n = 6$ and $l = 3$ is examined. For SWA, it has $\sigma = 0, 1, 2, 3$ subspaces. $\sigma = 0, 3$ are axes and $\sigma = 1, 2$ are planes. From (3), the mapping of the pole-voltage harmonics is as follows: $\sigma = 0, 2$ do not allow any valid q; $\sigma = 1$ has $q = 1, 7, -5, 13, \ldots$; and $\sigma = 3$ has $q = \pm 3, \pm 9, \pm 21, \ldots$ The mapping of phase and pole voltages is identical. For S6N1, $\sigma = 2, 3$ are the μ subspaces (see Table II), but since $\sigma = 2$ does not allow any valid q, it is ignored. Conversely, for S6N2, the current is prevented in $\sigma' = 3$, so μ is null. On the other hand, for AWA, the motor has $\sigma = 1, 3, 5$ planes. The mapping of the pole-voltage harmonics is as follows: $\sigma = 1$ has $q = 1, -11, 13, -23\ldots$; $\sigma = 3$, $q = 3, -9, 15, \ldots$; and $\sigma = 5$, $q = 5, -7, 17, \ldots$ For A6N1, $\sigma = 3, 5$ comprise the μ subspaces. Moreover, the mapping of pole and phase voltages differs for $\sigma' = 3$. The phase-voltage harmonic orders for $\sigma' = 3$ are $q = \pm 3, \pm 9, \pm 15, \ldots$ For A6N2, there is no current in $\sigma' = 3$, and hence, $\sigma = 5$ is the sole μ subspace.

B. Linear Region of PWM

To exploit the dc-link voltage in the linear PWM region, noncurrent-producing voltage harmonics are injected [9]. The min–max ZS injection is widely spread [9], [10]. For n-phase drives with one NP, the one ZS voltage is computed as a function of the reference voltage $\boldsymbol{v}$ as [9]

$$v_{\mathrm{zs}} = -0.5\left(\min(\boldsymbol{v}) + \max(\boldsymbol{v})\right) \tag{4}$$

increases to some extent the maximum value of modulation index M, where M is the ratio between the fundamental voltage peak and one half of the dc-link voltage. In general, said increment in achievable M tends to decay as n rises [10], [15]. Furthermore, one ZS injection yields no increment for even n with SWA since $v_{\mathrm{zs}} = 0$. Alternatively, in drives consisting of n/l winding sets with n/l NPs, either for SWA or AWA, one ZS per set (i.e., multiple ZSs) can be used to extend the linear region [5], [10]. Each ZS is computed as in (4), but only considering the phases comprising each set.

Overall, adding just ZS voltage does not take full advantage of the dc-link voltage [10]. This is overcome by additionally injecting low-order current-producing harmonics, achieved through operating the inverter in OVM. This allows reaching M beyond the linear region [16], [17].

III. RELATIONSHIP BETWEEN THE AMPLITUDES OF PHASE- AND POLE-VOLTAGE HARMONICS

The proposal achieves the MCD by injecting optimum pole-voltage harmonics. To this end, a certain cost function, calculated

by using the amplitudes of the pole-voltage harmonics, has to be minimized. Nonetheless, the current distortion is ultimately produced by the phase-voltage harmonics. Accordingly, it is necessary to establish a relationship between their amplitudes. Overall, the amplitudes of phase- and pole-voltage harmonics match, except in the special case noted earlier, i.e., for AWA with one NP. Although in Section II-A2, their subspace mapping is discussed, the relationship between their amplitudes is not well understood. This is clarified next before introducing the proposal.

The phase voltages for AWA with one NP are given by [26]

$$\boldsymbol{v}'' = \boldsymbol{v}' - \begin{bmatrix} 1 & 1 & \dots & 1 \end{bmatrix}^{\mathrm{T}} v_{\mathrm{NP}} \tag{5}$$

where $\boldsymbol{v}'$ is a vector containing balanced pole voltages, as

$$\boldsymbol{v}' = \begin{bmatrix} v'_{\mathrm{a}} & v'_{\mathrm{b}} & \cdots & v'_k & \cdots & v'_n \end{bmatrix}^{\mathrm{T}} \tag{6}$$

and v_{NP} is the voltage of a single NP, obtained as

$$v_{\mathrm{NP}} = \frac{1}{n}\sum_{k=1}^{n} v'_k. \tag{7}$$

By replacing (7) in (5), the latter can be rewritten as

$$\boldsymbol{v}'' = \left(\boldsymbol{I} - \frac{1}{n}\boldsymbol{J}\right)\boldsymbol{v}' \tag{8}$$

with $\boldsymbol{I}$ denoting the identity matrix, while $\boldsymbol{J}$ is a square matrix of ones. Then, the phase voltages $\boldsymbol{v}''$ are mapped into the σ subspaces, similarly to (2). Namely

$$\begin{bmatrix} \boldsymbol{v}''_{\boldsymbol{\alpha\beta},\mathbf{1}} & \boldsymbol{v}''_{\boldsymbol{\alpha\beta},\mathbf{3}} & \cdots & \boldsymbol{v}''_{\boldsymbol{\alpha\beta},\boldsymbol{\sigma}} & \cdots & \boldsymbol{v}''_{\boldsymbol{\alpha\beta},\boldsymbol{m}} \end{bmatrix}^{\mathrm{T}} = \boldsymbol{T}'\boldsymbol{v}' \tag{9}$$

where

$$\boldsymbol{T}' = \boldsymbol{T}\left(\boldsymbol{I} - \frac{1}{n}\boldsymbol{J}\right). \tag{10}$$

Note that (9) directly relates the pole voltages with the space vectors of phase voltages. $\boldsymbol{T}'$ is identical to $\boldsymbol{T}$ for subspaces (rows) other than $\sigma = \sigma'$. It follows that the amplitudes of phase-voltage harmonics match those of the pole ones for $\sigma \neq \sigma'$, whereas this is not necessarily satisfied for σ'. To find the relationship between their amplitudes for every $\sigma = \sigma'$, the following procedure is performed.

Each qth harmonic of $\boldsymbol{v}'$, with amplitude $\hat{v}_q$, is analyzed separately. Its initial phase angle is zeroed, since it does not affect the resulting amplitudes. Hence, every element in (6) is

$$v'_k = \hat{v}_q \cos\left(q(\theta - \phi_k)\right) \tag{11}$$

where θ is the instantaneous phase angle of the fundamental voltage component and ϕ_k is the spatial angle[1] between phase k and a. Expressing (11) by using complex notation results in

$$v'_k = \overbrace{\frac{\hat{v}_q}{2}\mathrm{e}^{\mathrm{j}|q|(\theta-\phi_k)}}^{\boldsymbol{v}'_{k+}} + \overbrace{\frac{\hat{v}_q}{2}\mathrm{e}^{-\mathrm{j}|q|(\theta-\phi_k)}}^{\boldsymbol{v}'_{k-}} \tag{12}$$

[1] ϕ_k equals the phase angle of the kth complex number in the vector $\boldsymbol{t}$ (see (A.3) in the Appendix).

TABLE III
RELATIONSHIP BETWEEN POLE- AND PHASE-VOLTAGE HARMONIC AMPLITUDES (c_q) IN σ' SUBSPACES FOR A6N1 WITH $l = 3$

σ'	qth pole-voltage harmonic	$\frac{\lvert\boldsymbol{v}''_{\boldsymbol{\alpha\beta},\mathbf{3}+}\rvert}{\hat{v}_q}$	$\frac{\lvert\boldsymbol{v}''_{\boldsymbol{\alpha\beta},\mathbf{3}-}\rvert}{\hat{v}_q}$
3	$3, 21, 39, \dots$	$1/2$	$1/2$
	$-15, -33, -51, \dots$	$1/2$	$1/2$

TABLE IV
RELATIONSHIP BETWEEN POLE- AND PHASE-VOLTAGE HARMONIC AMPLITUDES (c_q) IN σ' SUBSPACES FOR A9N1 WITH $l = 3$

σ'	qth pole-voltage harmonic	$\frac{\lvert\boldsymbol{v}''_{\boldsymbol{\alpha\beta},\mathbf{3}+}\rvert}{\hat{v}_q}$	$\frac{\lvert\boldsymbol{v}''_{\boldsymbol{\alpha\beta},\mathbf{3}-}\rvert}{\hat{v}_q}$	$\frac{\lvert\boldsymbol{v}''_{\boldsymbol{\alpha\beta},\mathbf{9}+}\rvert}{\hat{v}_q}$	$\frac{\lvert\boldsymbol{v}''_{\boldsymbol{\alpha\beta},\mathbf{9}-}\rvert}{\hat{v}_q}$
3	$3, 21, 39, \dots$	$5/9$	$4/9$	$1/9$	$1/9$
	$-15, -33, -51, \dots$	$4/9$	$5/9$	$1/9$	$1/9$
9	$9, 27, 45, \dots$	$2/9$	$2/9$	$4/9$	$4/9$

where the space vectors $\boldsymbol{v}'_{k+}$ and $\boldsymbol{v}'_{k-}$ have positive and negative sequences [27], respectively. By rewriting each element of (6) as in (12), and then, separating the space vectors rotating with positive and negative sequences into two arrays

$$\begin{aligned} \boldsymbol{v}'_{+} &= \begin{bmatrix} \boldsymbol{v}'_{\mathrm{a}+} & \boldsymbol{v}'_{\mathrm{b}+} & \cdots & \boldsymbol{v}'_{k+} & \cdots & \boldsymbol{v}'_{n+} \end{bmatrix}^{\mathrm{T}} \\ \boldsymbol{v}'_{-} &= \begin{bmatrix} \boldsymbol{v}'_{\mathrm{a}-} & \boldsymbol{v}'_{\mathrm{b}-} & \cdots & \boldsymbol{v}'_{k-} & \cdots & \boldsymbol{v}'_{n-} \end{bmatrix}^{\mathrm{T}}. \end{aligned} \tag{13}$$

Then, $\boldsymbol{v}'_{+}$ and $\boldsymbol{v}'_{-}$ are mapped into subspaces by using (9), as

$$\begin{aligned} &\begin{bmatrix} \boldsymbol{v}''_{\boldsymbol{\alpha\beta},\mathbf{1}+} & \boldsymbol{v}''_{\boldsymbol{\alpha\beta},\mathbf{3}+} & \cdots & \boldsymbol{v}''_{\boldsymbol{\alpha\beta},\boldsymbol{\sigma}+} & \cdots & \boldsymbol{v}''_{\boldsymbol{\alpha\beta},\boldsymbol{m}+} \end{bmatrix}^{\mathrm{T}} \\ &\quad = \boldsymbol{T}'\boldsymbol{v}'_{+} \\ &\begin{bmatrix} \boldsymbol{v}''_{\boldsymbol{\alpha\beta},\mathbf{1}-} & \boldsymbol{v}''_{\boldsymbol{\alpha\beta},\mathbf{3}-} & \cdots & \boldsymbol{v}''_{\boldsymbol{\alpha\beta},\boldsymbol{\sigma}-} & \cdots & \boldsymbol{v}''_{\boldsymbol{\alpha\beta},\boldsymbol{m}-} \end{bmatrix}^{\mathrm{T}} \\ &\quad = \boldsymbol{T}'\boldsymbol{v}'_{-}. \end{aligned} \tag{14}$$

Then, the phase-voltage harmonic amplitudes $|\boldsymbol{v}''_{\boldsymbol{\alpha\beta},\boldsymbol{\sigma}+}|$ and $|\boldsymbol{v}''_{\boldsymbol{\alpha\beta},\boldsymbol{\sigma}-}|$ for $\sigma = \sigma'$ are computed using (11)–(14) from the pole-voltage harmonics. The former are found to be $c_q\hat{v}_q$; c_q is a constant for certain q, σ' and sequence, regardless of θ.

As in Section II-A2, the case of A6N1 with $l = 3$ is examined. For $\sigma = 1, 5$, the amplitudes of the phase-voltage harmonics match those of their corresponding pole-voltage ones. On the other hand, for $\sigma' = 3$, $|\boldsymbol{v}''_{\boldsymbol{\alpha\beta},\mathbf{3}+}| = |\boldsymbol{v}''_{\boldsymbol{\alpha\beta},\mathbf{3}-}| = c_q\hat{v}_q$, where $c_q = 1/2$ for any q, as summarized in Table III. For other common types of machines, e.g., A9N1 and A12N1 with $l = 3$, the c_q values for σ' are given in Tables IV and V, respectively. For both motors, $\sigma' = 3, 9$ are coupled and any qth pole-voltage harmonic in them yields phase-voltage harmonics of order $\pm|q|$ for each $\sigma' = 3, 9$. Motors with $n > 12$ or $l \neq 3$ are uncommon in practice, but the c_q values can also be computed for them following this procedure.

As aforesaid, the preceding procedure is unnecessary for motors other than AWA and one NP since in them phase- and pole-voltage amplitudes always match.

TABLE V
RELATIONSHIP BETWEEN POLE- AND PHASE-VOLTAGE HARMONIC AMPLITUDES (c_q) IN σ' SUBSPACES FOR A12N1 WITH $l = 3$

σ'	qth pole-voltage harmonic	$\frac{\lvert v''_{\alpha\beta,3+}\rvert}{\hat{v}_q}$	$\frac{\lvert v''_{\alpha\beta,3-}\rvert}{\hat{v}_q}$	$\frac{\lvert v''_{\alpha\beta,9+}\rvert}{\hat{v}_q}$	$\frac{\lvert v''_{\alpha\beta,9-}\rvert}{\hat{v}_q}$
3	$3, 17, 51, \ldots$	0.5732	0.4268	0.1768	0.1768
	$-21, -45, -69, \ldots$	0.4268	0.5732	0.1768	0.1768
9	$9, 33, 57, \ldots$	0.1768	0.1768	0.9268	0.0732
	$-15, -39, -63, \ldots$	0.1768	0.1768	0.0732	0.9268

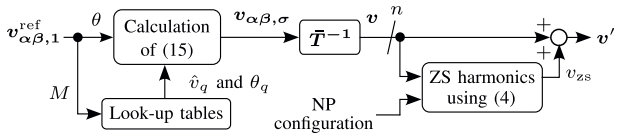

Fig. 1. Online implementation of the proposed method.

IV. GENERALIZED OVM METHOD WITH MCD FOR n-PHASE INDUCTION MOTOR DRIVES

For a given voltage reference $v^{ref}{}_{\alpha\beta,1}$ in OVM, the proposal must add the optimum balanced pole voltages at each sample to achieve the reference modulation index M while attaining the MCD. Two techniques are devised: MCD $_\mu$ and MCD$_{\alpha\beta\mu}$. MCD$_\mu$ injects only μ harmonics (see Table II), while MCD$_{\alpha\beta\mu}$ also injects $\alpha\beta_1$ harmonics. The benefits gained by injecting $\alpha\beta_1$ harmonics are that the current THD is further reduced while allowing higher M up to the square waveform ($M = 1.27$) [16], at the expense of some (small) increase in torque ripple. Both techniques have an offline and an online part. In the former, for each M, an optimization problem is solved to find the optimum amplitudes $\hat{v}_q$ and initial phase angles θ_q of the q th current-producing pole-voltage harmonics to be injected. They are stored in lookup tables and used in the online stage. For convenience, the online part is discussed first.

A. Online Implementation

Fig. 1 shows the online scheme, whose input is $v^{ref}{}_{\alpha\beta,1}$, containing just the desired fundamental voltage. To achieve the reference M with MCD, MCD$_{\alpha\beta\mu}$ and MCD$_\mu$ inject the appropriate harmonics at each sample as

$$v_{\alpha\beta,\sigma} = \sum_{q\in\alpha\beta_\sigma}^{|q|<Q} \hat{v}_q e^{jq(\theta-\theta_q)} \tag{15}$$

where Q is the absolute value of the highest order harmonic to be injected. Q is chosen at the offline stage, as discussed shortly. Only the voltages $v_{\alpha\beta,\sigma}$ of the current-producing subspaces are found by using (15), whereas the other ones are, in principle, zeroed. For the particular case of MCD$_\mu$ and $\sigma = 1$, only $q = 1$ is considered. For σ axes, just the real part of $e^{jq(\theta-\theta_q)}$ is relevant ($v_{\beta,\sigma} = 0$). Since this real part is the same for both q sequences, only the positive one is included at this stage in the summation for simplicity.

In Fig. 1, after using (15), and then, applying the inverse of the real-valued vector space decomposition matrix $\bar{T}$, given in the Appendix, v is obtained. Finally, one (for one NP) or n/l (for n/l NPs) ZSs are added by using (4), resulting in the optimum inverter pole-voltage references v'. The last step is unnecessary for even n with SWA and one NP, because $v' = v$.

As aforesaid, the lookup tables with the optimum $\hat{v}_q$ and θ_q values per M are the outcome of an offline optimization to minimize the current THD. This is analyzed next.

B. Offline Constrained Optimization Problem

1) Cost Function J: The current THD, resulting from adding pole-voltage harmonics by using (15), can be estimated through the voltage weighted THD (WTHD) by using $\hat{v}_q$. Note that certain nonidealities (e.g., dead-time harmonics) may influence the current distortion to some extent. Nevertheless, the effects of these nonideal factors on the current distortion are relatively minor compared with those caused by the injection of low-order harmonics to the voltage reference within the OVM range, and hence, the influence of the former on the current THD is not significant and can be neglected [11], [12], [24], as done subsequently. Under this assumption, minimizing the WTHD implies minimizing the current THD. For induction motor drives, the definition of the WTHD was enhanced in [16] to distinguish between planes and between frequencies. It is valid only for five-phase drives [16], but it is extended here to other ones

$$\mathrm{WTHD}^2 = \frac{1}{\hat{v}_1^2}\overbrace{\left(\sum_{1<q\in\alpha\beta_1}^{|q|<Q}\left(\frac{\hat{v}_q}{q}\right)^2 + \sum_{\sigma\in\mu}\delta_\sigma^2\sum_{q\in\alpha\beta_\sigma}^{|q|<Q}\left(\frac{c_q\hat{v}_q}{q}\right)^2\right)}^{J} \tag{16}$$

where δ_σ is a factor that reflects the large current distortion produced by the voltage harmonics of the μ subspaces, which is much greater than that produced by the $\alpha\beta_1$ ones [16]. Namely, δ_σ is the ratio between the $\alpha\beta_1$ transient stator inductance and the $\sigma \in \mu$ stator leakage inductance. The latter inductance is identical for any $\sigma \in \mu$ in motors with perfectly sinusoidal winding distribution [1]. Achieving this in practice is complex, leading to differences in the stator leakage inductances across each σ [28], [29]. Concerning the c_q values in (16), they are set as follows. For SWA with 1 or n/l NPs, and for AWA with n/l NPs: $c_q = 1$ for σ planes and $c_q = 1/2$ for σ axes, regardless of q. The latter is because using (15) then yields two pole voltages with sequences $\pm|q|$ (see Section II-A2) with the same amplitude of $\hat{v}_q/2$ [27]. For AWA and one NP: $c_q = 1$ for any q in $\sigma \neq \sigma'$ subspaces; for σ' subspaces the summation is carried out with the q values corresponding to the phase-voltage harmonic mapping (see Section II-A2), along with their respective c_q for each σ' and sequence (see Section III).

To achieve the MCD per M, the new cost function J [see (16)] has to be minimized. Unlike the cost function introduced in [[16], eq. (12)], J accurately estimates the current distortion, even when there is coupling between subspaces (for AWA with one NP) or when the effects of the nonideal winding distribution arise (through δ_σ). Note that J depends on Q. A large Q allows

higher M and lower current THD [16]. However, a large Q may also enlarge the lookup tables, and thus, increase the memory requirements [16]. Devising a general formula for determining Q, applicable across diverse winding configurations, is challenging. Nonetheless, a straightforward approach to set a suitable Q is suggested. It is based on gradually increasing Q until the reduction of THD and increase of M are marginal.

2) Constraints: Two main restrictions must be met while minimizing J. First, to attain the desired M, the fundamental voltage amplitude $\hat{v}_1$ should equal that of ${\boldsymbol{v}^{\text{ref}}}_{\boldsymbol{\alpha\beta},\mathbf{1}}$. Furthermore, θ_1 is set to zero since it does not influence the online part. Second, $\boldsymbol{v}'$, normalized by one half of the dc-link voltage, should be within ± 1 p.u. To enforce this constraint while minimizing J, $\boldsymbol{v}'$ is computed for one fundamental period with θ steps of $2\pi/(3Q)$ by following the scheme of Fig. 1. The lookup tables in Fig. 1 are not available yet; instead, an adequate optimization algorithm should iteratively search for the optimum $\hat{v}_q$ and θ_q, which are finally stored in lookup tables. The recommended offline sampling rate of $2\pi/(3Q)$, higher than the offline Nyquist frequency π/Q, provides enough resolution with acceptable complexity to ensure that $\boldsymbol{v}'$ will actually be within ± 1 p.u. after commissioning. Moreover, the online sampling during the drive operation must be at least $2f_1Q$, where f_1 is the fundamental frequency [16].

The optimization is solved in MATLAB by using the *GlobalSearch* algorithm, which runs the *fmincon* algorithm with the *sqp* solver. Initially, all unknowns are zeroed. For a given M and Q, MATLAB scripts of the offline optimization and the online implementation of MCD$_\mu$ and MCD$_{\alpha\beta\mu}$ for S6N1, S6N2, A6N1, and A6N2 are provided in the supplementary material of this article.

The proposed optimization problem is much simpler than that in [16] (just for $n = 5$). The latter involves numerous samples of a phase signal, whereas the proposal directly optimizes only the amplitude and initial phase angle of the pole harmonics. This improvement makes it general for any n, and facilitates the offline stage using far fewer variables and constraints. For instance, for S5N1 and $Q = 27$, minimizing J for MCD$_\mu$ optimizes 12 variables (six $\hat{v}_q$ and six θ_q) and uses three constraints, instead of 400 variables with five constraints as in [16]. Moreover, the lack of the Fourier transform, needed in [16], also expedites the offline stage. Nevertheless, although the offline part of the proposal is simpler than that of [16], the most important contribution is its generality.

V. Assessment of Current THD in Multiple Cases

Next, the current THD of the proposal is compared with that of the existing techniques. The most common types of n-phase machines and their potential NPs are considered. Among the motors that may have n/l NPs, only $l = 3$ is taken into account, since it is preferred in industrial applications [30], [31]. Space harmonics are neglected. Assuming that the stator transient inductance is roughly the sum of the stator and rotor leakage inductances [32], and considering the typical values of the ratio between the leakage inductances [33], it follows that δ_σ is often in the range of 2 to 3, roughly. Thus, $\delta_\sigma = 3$ is here set for all μ subspaces, although it has also been checked that the findings are consistent for other δ_σ. A sampling frequency of 10 kHz is used [12], [16], [18]. The current THD is estimated by the voltage WTHD [11], [24] as in (16), but considering all the harmonic orders below the Nyquist frequency (5 kHz). The switching effects are neglected [11].

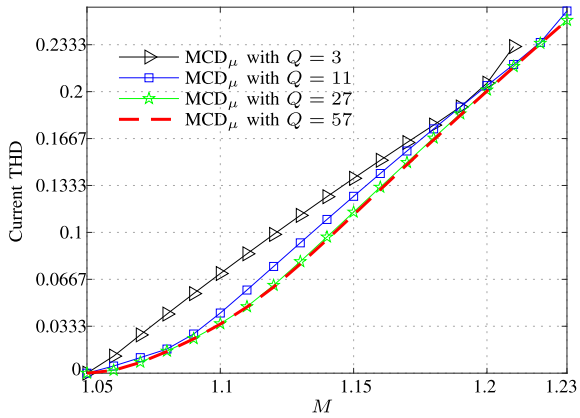

Fig. 2. Current THD (voltage WTHD) of MCD$_\mu$ for S5N1.

As already stated, the performance of the proposal depends on Q. The behavior of MCD$_\mu$ as Q rises is shown in Fig. 2 for S5N1, where a higher Q allows a lower current THD and greater M. Note that the reduction of current THD and increase of M are noticeable as Q increases up to $Q = 27$. However, for $Q > 27$, e.g., $Q = 57$, such reduction is almost negligible beyond that achieved by $Q = 27$. Since setting $Q = 57$ involves greater lookup tables and online sampling frequency than setting $Q = 27$, the latter value is chosen as it provides a satisfactory performance with less complexity. Note that, if there are limitations preventing the control board to cope with the memory resources or the online sampling frequency, a smaller Q may be set, while still achieving an acceptable performance. For example, setting a relatively lower $Q = 11$ for MCD$_\mu$ also attains a satisfactory low current THD (see Fig. 2), close to that reached by $Q = 27$, but with less computational resources. This procedure based on progressively increasing Q until achieving the desired performance can be performed for each machine type. The optimization is solved with M steps of 0.01.

Table VI summarizes the main features of the approaches to be compared. These features are supported by the quantitative data provided by the theoretical assessment discussed next and by the experiments in Section VI-B. The methods in [16] that minimize the current THD just for S5N1 are termed MCD-S5N1; those from [10], [14] and [15] based on only two large space vectors are labeled SV0; the space-vector method [13] that uses $n - 1$ space vectors whose duty cycles are set to avoid zero voltage vectors is termed SV1; the space-vector technique [12] that uses a sequential optimization to synthesize μ voltages is referred to as SV2; and the method in [21] that minimizes the voltage THD is labeled as MVD. SV1, SV2, and MVD are just for SWA with odd n. Although SV0 is suitable for any n, it produces a substantial THD [12], [13], and thus, it is only considered when there is no existing strategy to mitigate the

TABLE VI
MAIN CHARACTERISTICS OF PREVIOUS METHODS AND THE PROPOSED MCDS AND RESULTS OF THE PERFORMANCE ASSESSMENTS

References	Label	Method description	n	SWA/ AWA	NPs	Current THD	Full dc-link utilization
[16]	MCD-S5N1	Minimization of current THD	5	SWA	1	Minimum	Yes
[10], [14], [15]	SV0	Use only the two nearest large space vectors	Any†	Any	Any	Very High	No
[13]	SV1	Avoid zero voltage vectors	Odd	SWA	1	High	No
[12]	SV2	Sequential optimization	≥ 7 (odd)	SWA	1	Medium	No
[5]	SV-A6	Minimization of voltage THD	6	AWA	2	Low	No
[21]	MVD	Minimization of voltage THD	Odd	SWA	1	Low	No
Proposed here	MCD_{μ}	Minimization of current THD while injecting μ harmonics	Any†	Any	Any	Minimum	No
Proposed here	$\text{MCD}_{\alpha\beta\mu}$	Minimization of current THD while injecting μ and $\alpha\beta_1$ harmonics	Any	Any	Any	Minimum	Yes

† Not suitable for S6N2 since μ is null.

THD. For AWA, there is only one previous technique for $n = 6$ [5] with low THD, termed as SV-A6.

A. Assessment for SWAs

The SWA assessment is divided regarding the NPs.

1) SWAs With One NP: The current THDs (voltage WTHDs) for several n are depicted in Fig. 3. It also includes the Q values for the novel MCDs. For odd n, SV1 produces the largest THD, followed by SV2, with an acceptable one, but unsuitable for S5N1. However, SV1 and SV2 deviate notably from the minimum current THD, established by the MCDs. The THDs of MVD are the closest to those of the MCDs. Unlike SV1, SV2, and MVD, the MCDs are also applicable for even n (see Fig. 3). Indeed, there is no strategy other than the new MCDs to alleviate the THD of SV0 for these motors. Although $n = 6, 9, 12$ with SWA can have $n/3$ NPs, setting a single NP offers enhanced tolerance for open-phase faults [8]; this reinforces the need for the new MCDs. The proposed MCDs offer significant advantages over existing techniques, but it is necessary to discuss the differences between them. For S6N1 in Fig. 3(b), $\text{MCD}_{\alpha\beta\mu}$ greatly reduces the THD compared with SV0, or even with MCD_{μ}, while it attains M up to 1.27. These advantages diminish as n rises, e.g., for S11N1 in Fig. 3(e), where the THD and the maximum M of $\text{MCD}_{\alpha\beta\mu}$ are similar to those of MCD_{μ}. This is because, as n increases, the $\alpha\beta_1$ plane has relatively higher order harmonics [see (3)], which are less effective for reaching higher M or lower current THD than injecting only μ voltage. It is also verified that the new MCDs are equivalent to those of MCD-S5N1 for S5N1 in Fig. 3(a). In fact, it has been checked that the experimental results by employing the new MCDs match those of MCD-S5N1.

2) SWAs With $n/3$ NPs: The current THD versus M in OVM for $n/3$ NPs are illustrated in Fig. 4. Setting $n/3$ NPs permits extending the linear region of PWM up to 1.15 by injecting multiple ZSs [10], [24]. For S6N2, μ is null (see Section II-A2), and OVM is performed by injecting only $\alpha\beta_1$ harmonics, as $\text{MCD}_{\alpha\beta\mu}$ does. For S9N3, SV1 still produces considerable THD. Compared with S9N1, the relationship between SV2 and MVD becomes more complex for S9N3: now SV2 produces less THD than MVD for $M \leq 1.19$, whereas for $M > 1.19$ this situation is reversed. The reason is that MVD minimizes the voltage THD taking into account, apart from the harmonics of the μ subspaces,

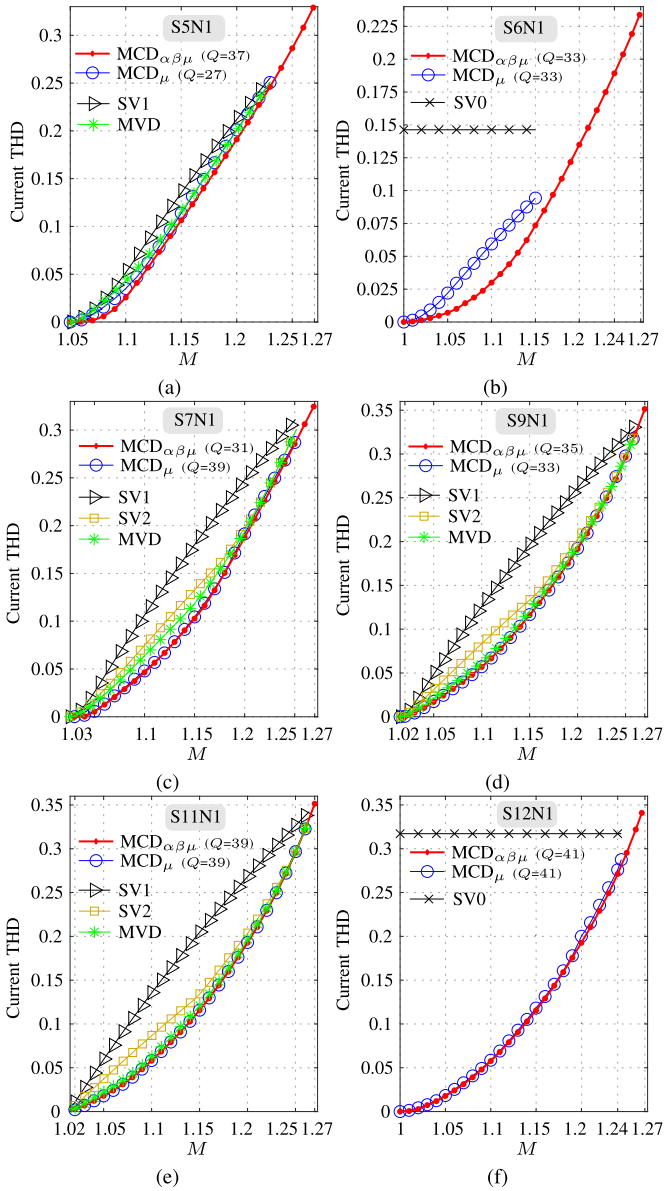

Fig. 3. Comparison of current THD (voltage WTHD) versus M in (a) S5N1, (b) S6N1, (c) S7N1, (d) S9N1, (e) S11N1, and (f) S12N1.

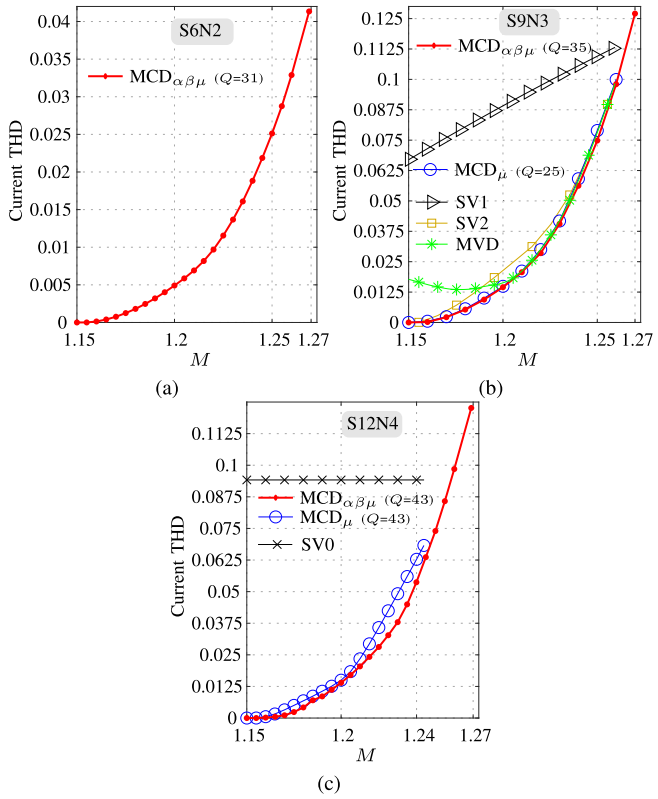

Fig. 4. Comparison of current THD (voltage WTHD) versus M in (a) S6N2, (b) S9N3, and (c) S12N4.

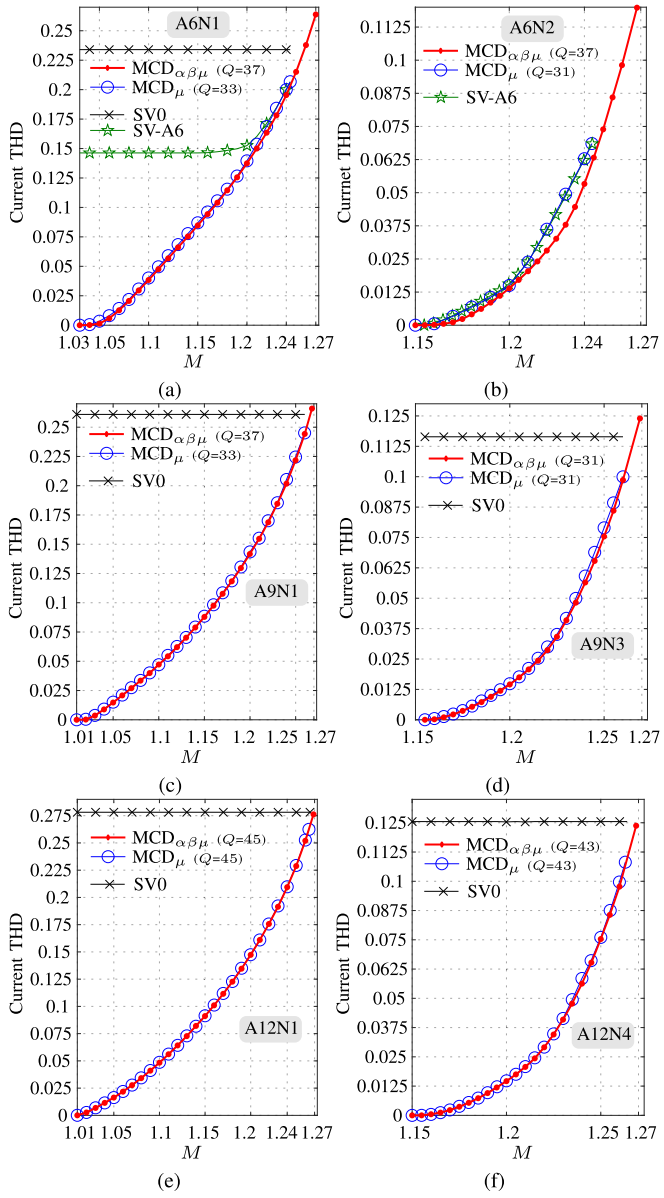

Fig. 5. Comparison of current THD (voltage WTHD) versus M in (a) A6N1, (b) A6N2, (c) A9N1, (d) A9N3, (e) A12N1, and (f) A12N4.

those of the subspaces in which the current is restricted due to the $n/3$ NPs. In consequence, current harmonics are caused even for $M \leq 1.15$ (linear region). In contrast to MVD, for $M \leq 1.19$, SV2 injects mainly a third-order voltage harmonic, and therefore, yields less THD than MVD. For higher M, both SV2 and MVD get closer to the minimum current THD, established by the MCDs. For S12N4, the only previous technique is SV0, which produces a large THD. The performance of MCD$_{\mu}$ and MCD$_{\alpha\beta\mu}$ is consistent as they produce a striking reduction of THD compared with SV0. Furthermore, besides attaining the square waveform, MCD$_{\alpha\beta\mu}$ offers an additional advantage over MCD$_{\mu}$ for $M > 1.22$ in terms of THD. Although $n = 12$ is relatively large, the $\alpha\beta_1$ plane still has low-order voltage harmonics, e.g., $q = -11, 13$ [given by (3)], which are useful to decrease the THD even more than MCD$_{\mu}$. While S12N1 also exhibits these $\alpha\beta_1$ harmonics, the advantage is more evident in S12N4 due to the large THD caused by the third μ harmonic in the former.

B. Assessment for AWAs

For AWAs, the only previous method, just for $n = 6$, is SV-A6. It was devised for A6N2, as in Fig. 5(b), but it is also evaluated for A6N1 in Fig. 5(a). For A6N1, SV-A6 yields lower current THD than SV0, but it gives much more THD than the MCDs for most M. For A6N2, SV-A6 reaches the THD of MCD$_{\mu}$, but it is greater than that of MCD$_{\alpha\beta\mu}$, especially for $M > 1.2$. For $n > 6$, there is no method to alleviate the SV0 THD other than the new MCDs. They produce a striking THD reduction for these machines as well; see Fig. 5(c)–(f). The benefits of MCD$_{\alpha\beta\mu}$ over MCD$_{\mu}$ are small for $n > 6$: the THD and maximum M are nearly equal.

C. Summary

As summarized in Table VI, the proposed MCDs are advantageous over previous OVM techniques, as they attain the minimum current THD for any n and NPs, and for either SWA or AWA. Although a few existing techniques become closer to the benchmark provided by the MCDs, they are severely limited to specific n, SWA/AWA, and NPs.

For any machine, the maximum M by employing MCD$_{\mu}$ equals that of the techniques that inject only μ voltage, e.g.,

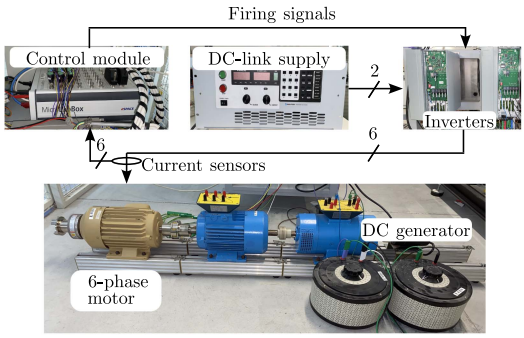

Fig. 6. Scheme and photographs of the experimental setup.

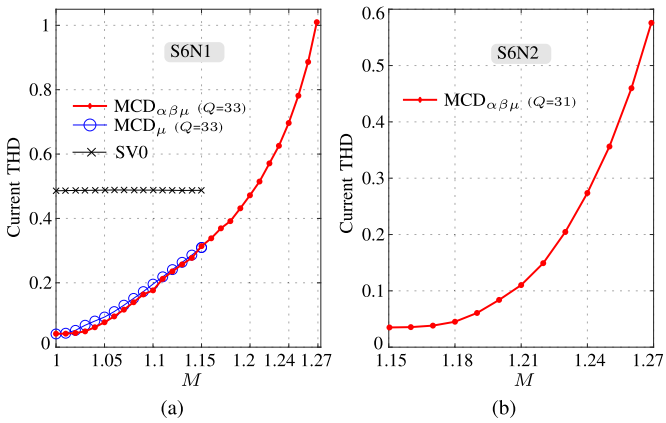

Fig. 7. Experimental current THD versus M for (a) S6N1 and (b) S6N2.

SV0. On the other hand, MCD$_{\alpha\beta\mu}$ achieves the best dc-link utilization, as it may attain the square waveform ($M = 1.27$).

VI. Experimental Results

A. Test-Bench Description

Two six-phase induction motors, one with SWA and the other with AWA, are employed for the experiments when one and two NPs are set. This is convenient for testing the adaptability of the proposal across different winding arrangements and neutral connections. Moreover, six-phase motors have attracted considerable attention as they provide several advantages. One of them is that it can be fed by using off-the-shelf three-phase inverters [8], thus avoiding the need for tailor-made hardware. Moreover, these motors can be straightforwardly obtained by rewinding three-phase stator frames [34]. For these reasons, these machines are widely used in industrial applications [2], e.g., electrified transportation [35] and aerospace applications [36]. Their main parameters are listed in Table VII. They have been obtained by rewinding two identical three-phase machines. Fig. 6 shows the experimental setup. The motor shaft is coupled to a dc generator through an unconnected motor that serves as a mechanical link. The test-bench inertia is 0.02 kg $\cdot$ m^2. The speed is measured by a tachometer, while the electromagnetic torque is estimated from the current measurements and a stator-flux observer as in [37]. They are supplied by two three-phase inverters with

TABLE VII
Main Parameters of the Six-Phase Motors for the Experiments

Parameter	SWA	AWA
Pole pairs	1	1
Stator resistance (Ω)	6.9	6.7
Rotor resistance (Ω)	6.3	7
Stator leakage inductance of $\sigma = 1$ (mH)	4.6	5.85
Stator leakage inductance of $\sigma = 3$ (mH)	45.3	40.7
Stator leakage inductance of $\sigma = 5$ (mH)	–	8.6
Rotor leakage inductance of $\sigma = 1$ (mH)	59.7	55.7
Magnetizing inductance of $\sigma = 1$ (mH)	652	708.5
Transient stator inductance of $\sigma = 1$ (mH)	59.3	57.5
Rated voltage (V)	110	110
Rated current (A)	2.2	2.2
Rated frequency (Hz)	50	50
Rated torque (Nm)	3.4	3.5
Rated speed (r/min)	2360	2465

TABLE VIII
Total Count of Constants Stored in Lookup Tables by MCD$_{\mu}$ and MCD$_{\alpha\beta\mu}$ for the Experiments

	S6N1	S6N2	A6N1	A6N2
MCD$_{\mu}$	180	–	676	154
MCD$_{\alpha\beta\mu}$	896	330	1064	624

a switching frequency of 10 kHz and dead time of 2 μs. The inverters are controlled by the platform dSPACE MicroLabBox with a sampling frequency of 10 kHz. As in [5], [6], [17], and [25], to avoid harmonics due to inverter nonlinearities and for better assessment of the injected low-order voltage harmonics, the voltage signals refer to those of the inverter voltage references. The current signals are oversampled and averaged to reduce the undesired effects of switching noise and parasitic oscillations [10], [19], [38]. The current THDs are computed considering all the harmonic orders below the Nyquist frequency (5 kHz).

Similar to Section V, the lookup tables after solving the offline optimization for the new MCDs were obtained for M steps of 0.01. In (16), δ_σ is set according to the parameters from Table VII: $\delta_3 = 1.31$ for SWA, and $\delta_3 = 1.41$ and $\delta_5 = 6.68$ for AWA. S6N1, S6N2, A6N1, and A6N2 are considered, and the Q values for the novel MCDs are set as in Figs. 3–5. The total count of constants stored in lookup tables by the MCDs is summarized in Table VIII. Assuming a standard amount of 8 B for storing each constant, in the worst-case scenario in Table VIII, i.e., for MCD$_{\alpha\beta\mu}$ and A6N1, approximately 8.31 kB are needed, which does not pose a limitation even for available low-cost control platforms.

The feasibility of the novel MCDs is validated by experiments in steady state in Section VI-B and by speed transients in Section VI-C. The former are performed by using open-loop scalar *V/f*, while the latter, by speed closed-loop scalar *V/f* control. These scalar controllers are well-suited for OVM since they inject harmonics in the voltage references without needing complex inner closed-loop current controllers [39]. Additional advantages of open-loop scalar controllers include simplicity [30], independence of machine parameters [40], avoidance of speed/position sensors or estimation algorithms [30], etc.

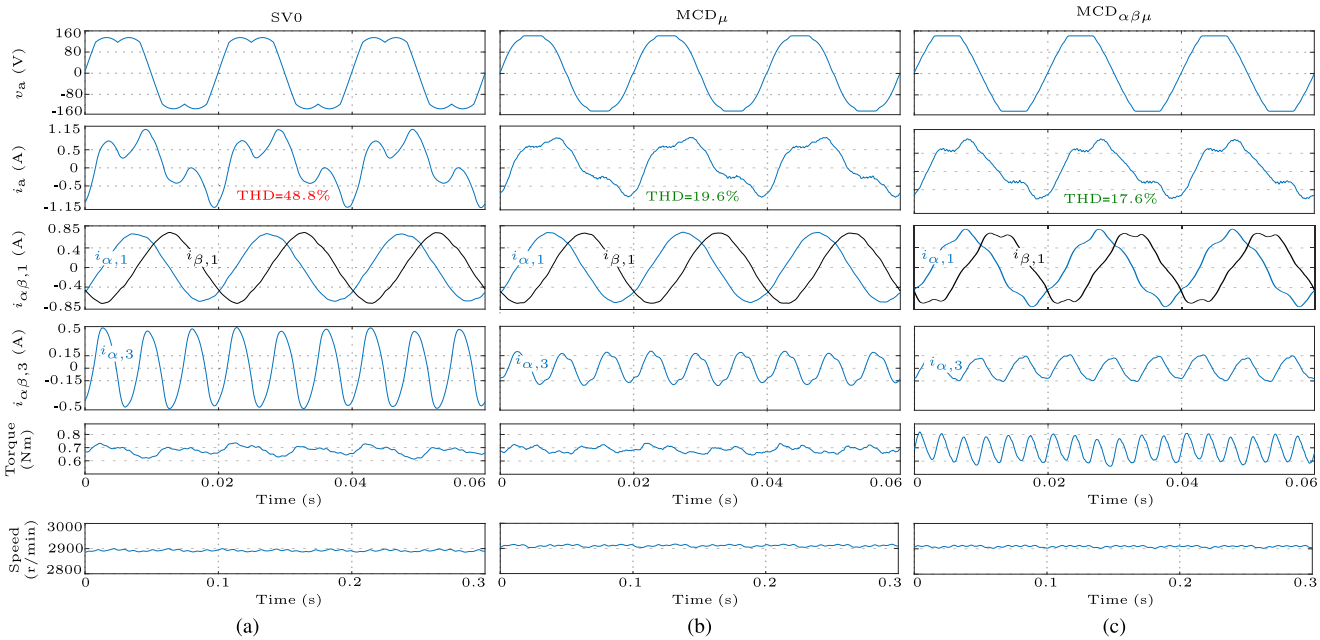

Fig. 8. Experimental results of S6N1 in the time domain of (a) SV0, (b) MCD$_\mu$, and (c) MCD$_{\alpha\beta\mu}$ for $M = 1.10$. From top to bottom: inverter pole-voltage reference of phase a v_a; current of phase a i_a; $\alpha\beta_1$ current; $\alpha\beta_3$ current; electromagnetic torque; and rotor speed.

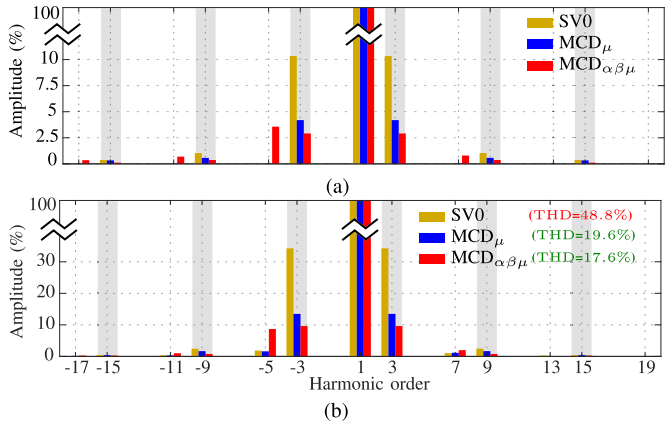

Fig. 9. Experimental spectra of S6N1 for $M = 1.10$ of the (a) phase-voltage references and (b) stator currents. The $\alpha\beta_3$ harmonics are shaded.

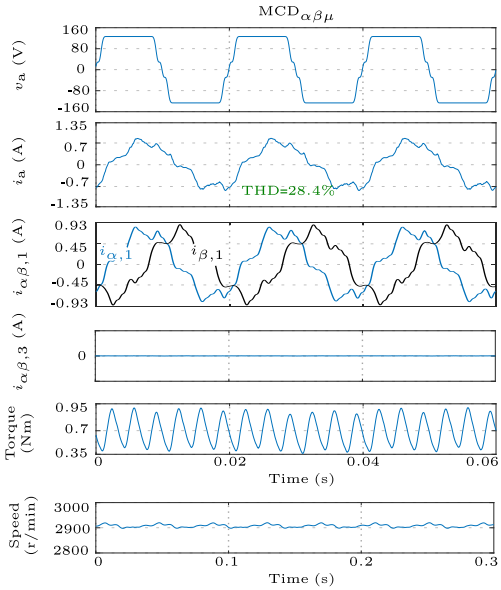

Fig. 10. Experimental results of S6N2 in the time domain of MCD$_{\alpha\beta\mu}$ for $M = 1.24$. From top to bottom: inverter pole-voltage reference of phase a v_a; current of phase a i_a; $\alpha\beta_1$ current; $\alpha\beta_3$ current; electromagnetic torque; and rotor speed.

B. Steady-State Experiments

The motors are driven by open-loop scalar *V/f*, maintaining their rated voltage (110 V) and rated frequency (50 Hz). Then, the dc-link voltage, initially equal to 306 V, is gradually decreased, as done in other papers [5], [6], [25]. This provides M in the OVM range, with a nearly constant fundamental current amplitude. Since the load condition has negligible effects on the harmonic currents [5], the tests are performed without load to avoid overheating risk.

1) Experiments With S6N1: The experimental current THDs for the OVM methods adequate for S6N1 are shown in Fig. 7(a). The current–THD plots are similar to those predicted in Fig. 3(b), although their absolute values differ due to the normalization by the fundamental current. Even though the actual THDs include some nonidealities, e.g., dead-time harmonics, they resemble the WTHD computed in Fig. 3(b) by (16), which does not take these nonidealities into account. This supports the fact that the current distortion in OVM is mainly due to the injection of low-order harmonics. As expected, SV0 produces a considerable current distortion. Conversely, the proposed MCDs

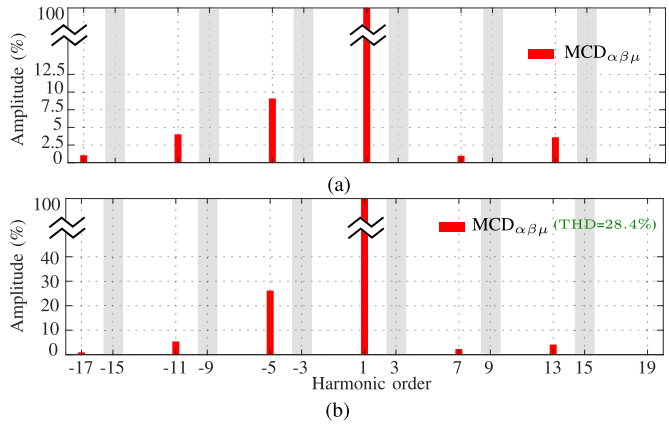

Fig. 11. Experimental spectra of S6N2 for $M = 1.24$ of the (a) phase-voltage references and (b) stator currents. The $\alpha\beta_3$ harmonics are shaded.

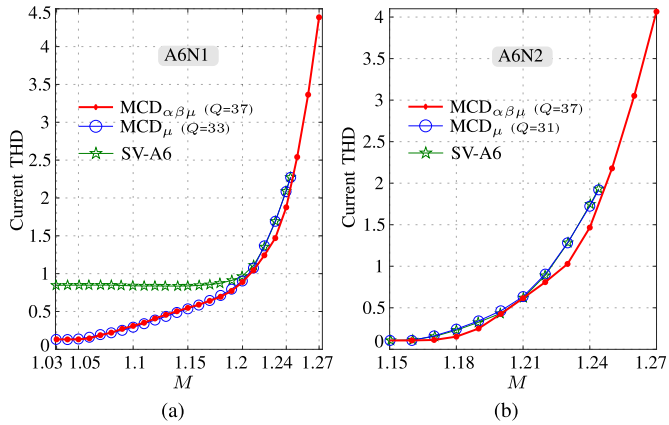

Fig. 12. Experimental current THDs versus M for (a) A6N1 and (b) A6N2.

attain a remarkable reduction. Compared with Fig. 3(b), the advantage of MCD$_{\alpha\beta\mu}$ over MCD$_{\mu}$ in THD is relatively small because of the existence of space harmonics, which increase to some extent the impedance for $\sigma = 3$ [29], which contains mainly the third harmonic. Therefore, for this particular motor, favoring the injection of $\alpha\beta_1$ harmonics over $\alpha\beta_3$ ones is less advantageous to reduce the current distortion. Nonetheless, MCD$_{\alpha\beta\mu}$ achieves M up to the square waveform.

Several measurements for $M = 1.10$ are illustrated for SV0, MCD$_{\mu}$, and MCD$_{\alpha\beta\mu}$ in Fig. 8. SV0 yields the greatest current THD of 48.8%, whereas those of MCD$_{\mu}$ and MCD$_{\alpha\beta\mu}$ are significantly lower: 19.6% and 17.6%, respectively. Note that, for lower M, the advantage of the MCDs over SV0 is even greater [see Fig. 7(a)]. For any method, the torque-producing $\alpha\beta_1$ currents are almost sinusoidal, although some distortion can be observed for MCD$_{\alpha\beta\mu}$, so as to reduce the phase-current THD. Concerning the $\alpha\beta_3$ current, that of SV0 is notably large. Conversely, MCD$_{\mu}$ greatly reduces this current, which is further mitigated by MCD$_{\alpha\beta\mu}$. Some distortion arises in the torque for SV0 and MCD$_{\mu}$, although they do not inject torque-producing harmonics. This almost negligible distortion is mainly caused by inverter and motor nonidealities [28]. On the other hand, small sixth-order oscillations appear for MCD$_{\alpha\beta\mu}$, but they do not cause noticeable effects on the rotor speed, which is similar to that of SV0 or MCD$_{\mu}$. Arguably, in low-inertia systems where torque ripple may cause speed oscillations [41], MCD$_{\mu}$ may be considered the best choice since it prevents the injection of torque-producing harmonics while ensuring low current THD.

Fig. 9(a) and (b) depicts the spectra, normalized by their fundamental amplitudes, of the phase-voltage references and the stator currents, respectively, for $M = 1.10$. From Fig. 9(a), SV0 mainly injects a large third harmonic, which is significantly reduced by MCD$_{\mu}$. MCD$_{\alpha\beta\mu}$ diminishes even more this harmonic by injecting instead a $\alpha\beta_1$ fifth one, with a larger impedance. This effectively alleviates the current THD. The current spectrum illustrated in Fig. 9(b) is analogous to that of Fig. 9(a), although some $\alpha\beta_1$ fifth and seventh harmonics appear for SV0 and MCD$_{\mu}$ due to the nonidealities.

2) Experiments With S6N2: The current THDs of MCD$_{\alpha\beta\mu}$ for S6N2 are shown in Fig. 7(b), which resemble those of Fig. 4(a). As aforesaid, MCD$_{\alpha\beta\mu}$ exploits the dc-link voltage up to $M = 1.27$.

Fig. 10 shows some measurements for a relatively high M: $M = 1.24$ where the current THD is 28.4%. The $i_{\alpha\beta,1}$ components show some acceptable distortion, which is unavoidable for the entire OVM range of S6N2 since $i_{\alpha\beta,3}$ is restricted to zero due to the two NPs. This yields small torque pulsation of sixth order, without noticeable influence on speed.

The spectrum of the phase-voltage references [see Fig. 11(a)] is analogous to that of the stator currents [see Fig. 11(b)] for $M = 1.24$. It can be noticed that MCD$_{\alpha\beta\mu}$ mainly injects a fifth-order harmonic to achieve such M.

3) Experiments With A6N1: For A6N1, apart from the proposed MCDs, SV-A6 is considered, whereas SV0 is now disregarded since it produces much more distortion than SV-A6, as discussed earlier. The current THD versus M is illustrated in Fig. 12(a), which is in good agreement with that estimated in Fig. 5(a), although their absolute values also differ for the aforementioned reason. Nonetheless, some reasonable discrepancies between these figures appear, e.g., the THD dramatically increases for $M > 1.20$ for all techniques in Fig. 12(a). These discrepancies are mainly caused by the parasitic space harmonics, which lead to notable differences between δ_3 and δ_5 (see Table VII). In particular, SV-A6 yields a nearly constant current THD for M below 1.20, which is much greater than that of the MCDs, especially for relatively low M. For $M > 1.20$, SV-A6 reaches the reduced current THD of MCD$_{\mu}$, but still produces more distortion than MCD$_{\alpha\beta\mu}$. On the other hand, the THDs of MCD$_{\mu}$ and MCD$_{\alpha\beta\mu}$ are similar for $M < 1.20$, whereas for $M > 1.20$, MCD$_{\alpha\beta\mu}$ is more advantageous over MCD$_{\mu}$.

Some measurements for SV-A6, MCD$_{\mu}$, and MCD$_{\alpha\beta\mu}$ are illustrated in Fig. 13 for $M = 1.10$. The current THD of SV-A6 (83.9%) is notably mitigated by MCD$_{\mu}$ (29.5%) or MCD$_{\alpha\beta\mu}$ (30.6%). For this particular M, the current THD of MCD$_{\mu}$ is marginally less than that of MCD$_{\alpha\beta\mu}$ due to nonidealities, but this is negligible when compared with the substantial difference of THD between SV-A6 and the MCDs. For MCD$_{\alpha\beta\mu}$, $i_{\alpha\beta,1}$ has small 11th and 13th harmonics. Regarding $i_{\alpha\beta,3}$, for the

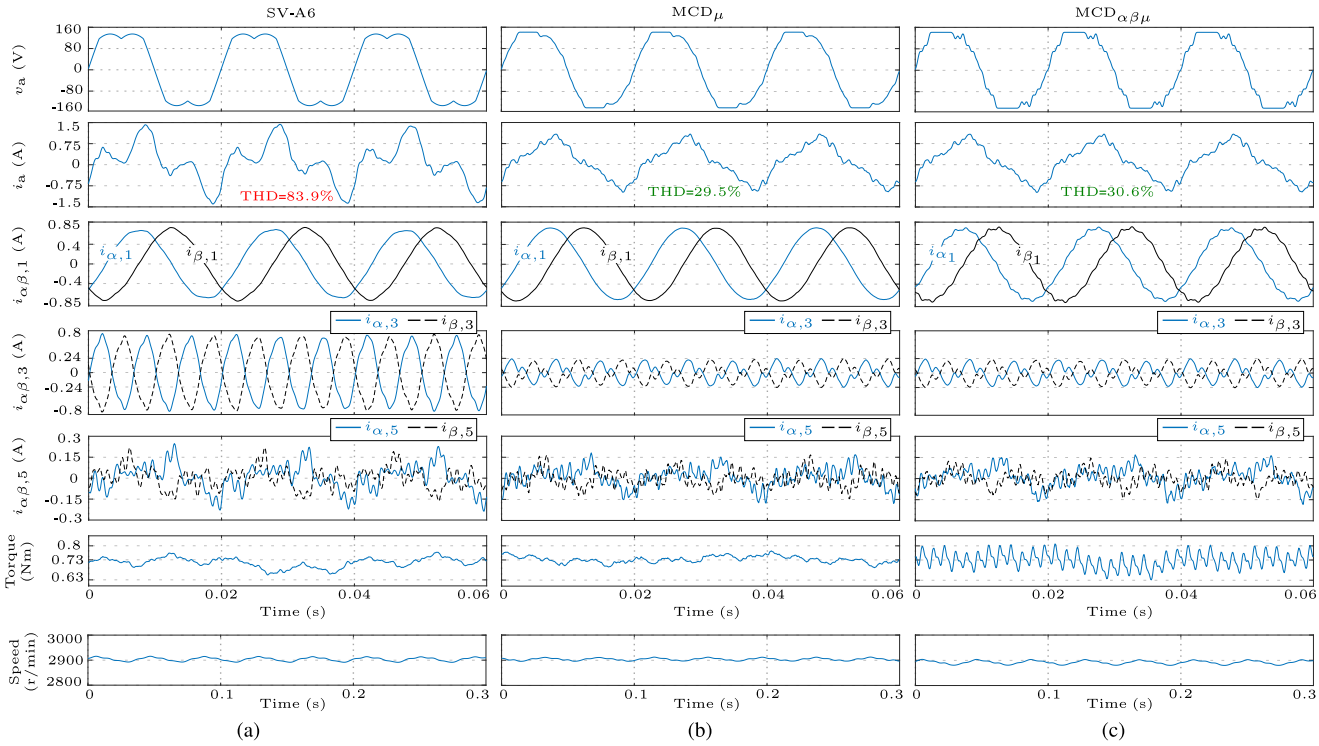

Fig. 13. Experimental results of A6N1 in the time domain of (a) SV-A6, (b) MCD$_\mu$, and (c) MCD$_{\alpha\beta\mu}$ for $M = 1.10$. From top to bottom: inverter pole-voltage reference of phase a v_a; current of phase a i_a; $\alpha\beta_1$ current; $\alpha\beta_3$ current; $\alpha\beta_5$ current; electromagnetic torque; and rotor speed.

MCDs, it is much smaller than for SV-A6. There are no major differences among the methods for $i_{\alpha\beta,5}$. Some negligible torque oscillations arise for SV-A6 and MCD$_\mu$ due to nonidealities, not to these techniques. Conversely, MCD$_{\alpha\beta\mu}$ leads to (small) torque ripple, mainly of 12th order. For any approach, whether or not $\alpha\beta_1$ harmonics are injected, no noticeable effects on the speed arise.

The reason behind the $i_{\alpha\beta,5}$ similarities (see Fig. 13) among the techniques and the rapid increase of current THD for $M > 1.20$ [see Fig. 12(a)] can be inferred by analyzing the voltage [see Fig. 14(a)] and current [see Fig. 14(b)] spectra. From Fig. 14(a), the new MCDs notably reduce the current-producing harmonics compared with SV-A6, especially for the $\alpha\beta_3$ third one, by injecting instead relatively greater higher order harmonics, with larger impedances, e.g., the ninth. Furthermore, note that SV-A6 and the MCDs mainly inject $\alpha\beta_3$ harmonics. For the MCDs, this is because the $\alpha\beta_3$ impedance is much greater than that of $\alpha\beta_5$ (see Table VII), so the injection in the latter is prevented. The current spectrum of Fig. 14(a) is similar to that of Fig. 12(a), disregarding a small amount of fifth and seventh components that appear for all methods, mainly caused by dead time. For these reasons, the $i_{\alpha\beta,5}$ waveforms shown in Fig. 13 are comparable for all techniques. Regarding the rapid increase of current THD for $M > 1.20$, it is mostly due to the unavoidable injection of large $\alpha\beta_5$ harmonics, which produce considerable currents. This fact is further investigated in the subsequent experiments. On the other hand, the injection of balanced pole-voltage harmonics in the $\sigma' = 3$ plane leads to phase-voltage harmonics [see Fig. 14(a)] having both sequences with the same amplitudes, as anticipated in Section III.

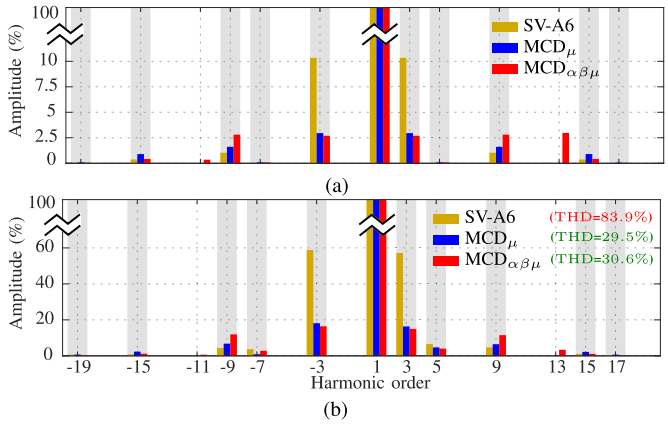

Fig. 14. Experimental spectra of A6N1 for $M = 1.10$ of the (a) phase-voltage references and (b) stator currents. The $\alpha\beta_3$ and $\alpha\beta_5$ harmonics are shaded.

4) Experiments With A6N2: By imposing two NPs, the excitation of the $\alpha\beta_3$ plane is prevented, and only the $\alpha\beta_1$ and $\alpha\beta_5$ harmonics can be injected. For A6N2, the current THD versus M is illustrated in Fig. 12(b). In contrast to the unsatisfactory performance shown for one NP, the performance of SV-A6 is now acceptable since it is close to the minimum current THD of MCD$_\mu$. On the other hand, MCD$_{\alpha\beta\mu}$, besides achieving $M = 1.27$, yields an additional advantage compared

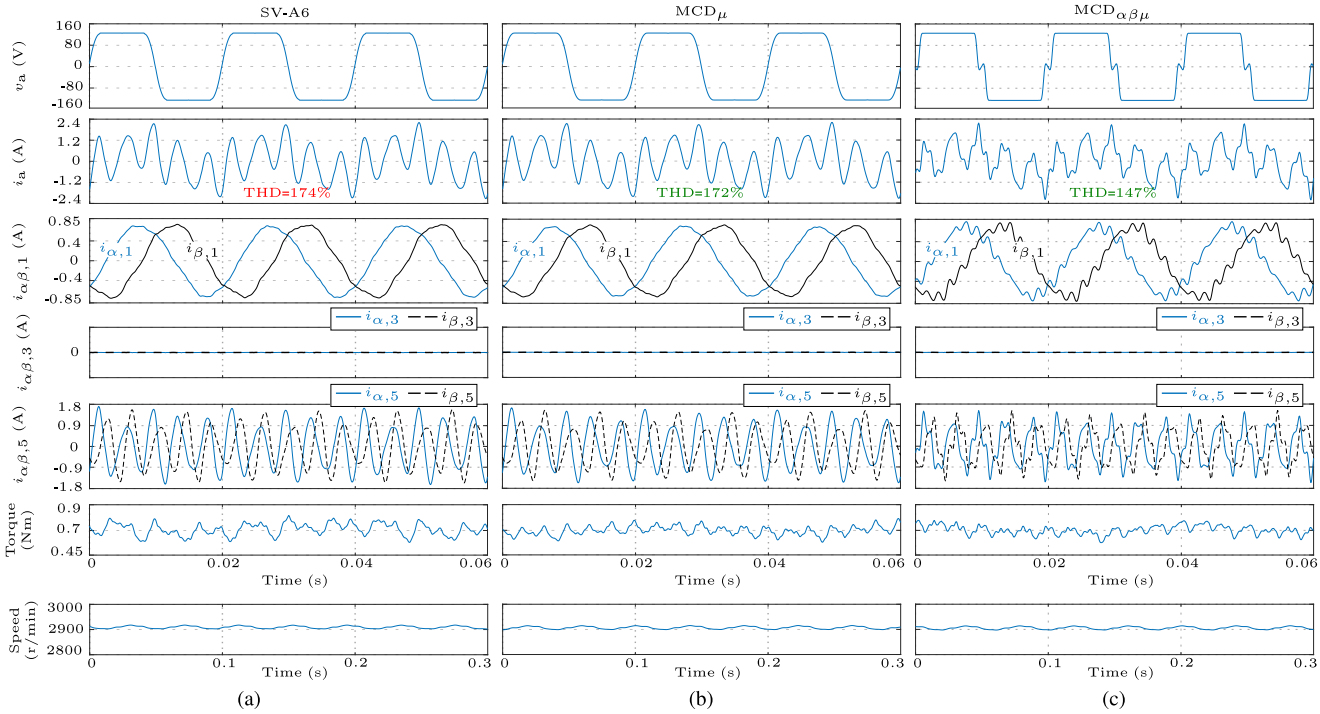

Fig. 15. Experimental results of A6N2 in the time domain of (a) SV-A6, (b) MCD$_\mu$, and (c) MCD$_{\alpha\beta\mu}$ for $M = 1.24$. From top to bottom: inverter pole-voltage reference of phase a v_a; current of phase a i_a; $\alpha\beta_1$ current; $\alpha\beta_3$ current; $\alpha\beta_5$ current; electromagnetic torque; and rotor speed.

with SV-A6 or even MCD$_\mu$ by further reducing the current THD, especially for $M > 1.21$.

As in preceding scenarios, several measurements are provided to assess the behavior of SV-A6, MCD$_\mu$ and MCD$_{\alpha\beta\mu}$, depicted in Fig. 15 for $M = 1.24$. The pole-voltage references of SV-A6 and MCD$_\mu$ are nearly the same, and both differ from MCD$_{\alpha\beta\mu}$. Thus, the phase currents of SV-A6 and MCD$_\mu$ are similar, although the THD of SV-A6 (174%) is slightly higher than that of MCD$_\mu$ (172%). On the contrary, the phase currents of MCD$_{\alpha\beta\mu}$ are less distorted, reducing the current THD down to 147%. $i_{\alpha\beta,1}$ of SV-A6 and MCD$_\mu$ are close to sinusoidal, whereas that of MCD$_{\alpha\beta\mu}$ exhibits a slight distortion. As a consequence of setting two NPs, $i_{\alpha\beta,3}$ is restricted to zero. Conversely, $i_{\alpha\beta,5}$ is large for SV-A6 and MCD$_\mu$, whereas MCD$_{\alpha\beta\mu}$ mitigates to some extent these currents. Concerning the torque, some small pulsations appear for all techniques, and therefore, no major differences exist in the speed.

For A6N2, the voltage and current spectra for $M = 1.24$ are shown in Fig. 16(a) and (b), respectively. SV-A6 and MCD$_\mu$ have a similar voltage spectrum, but the latter yields a smaller fifth harmonic (with low impedance), which reduces the current THD. Conversely, MCD$_{\alpha\beta\mu}$ greatly alleviates the $\alpha\beta_5$ injection by reducing the fifth harmonic and totally avoiding the seventh one. Instead, it injects higher-order $\alpha\beta_5$ harmonics, such as the 17th and 19th, and $\alpha\beta_1$ ones. Accordingly, as discussed earlier, MCD$_{\alpha\beta\mu}$ adds harmonics that see larger impedances to effectively decrease the current THD. The current spectrum of Fig. 16(b) reveals an extremely large fifth component for SV-A6 and MCD$_\mu$, which is attenuated by MCD$_{\alpha\beta\mu}$. Apart from the fifth harmonic, a noticeable seventh one for SV-A6 and MCD$_\mu$

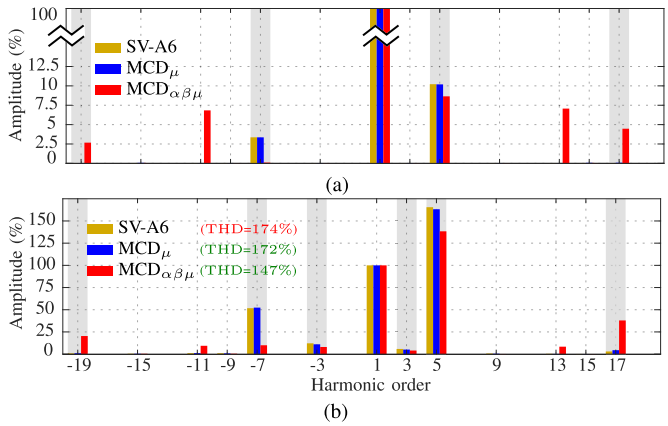

Fig. 16. Experimental spectra of A6N2 for $M = 1.24$ of the (a) phase-voltage references and (b) stator currents. The $\alpha\beta_5$ harmonics are shaded.

also contributes to the current distortion. Furthermore, the fifth harmonic is much larger than the fundamental component. In addition, although the flow of the $\alpha\beta_3$ third current harmonic is prevented due to the NP configuration, some relatively small content of this harmonic appears in $\alpha\beta_5$ for all methods. This is mainly caused by machine asymmetries, which are almost unavoidable in practice [34].

Based on the experimental results, the new MCDs are suitable for achieving the lowest current THD for motors with either SWA or AWA, independently of their NP configuration, thus supporting the features in Table VI and validating the theoretical assessment of Section V.

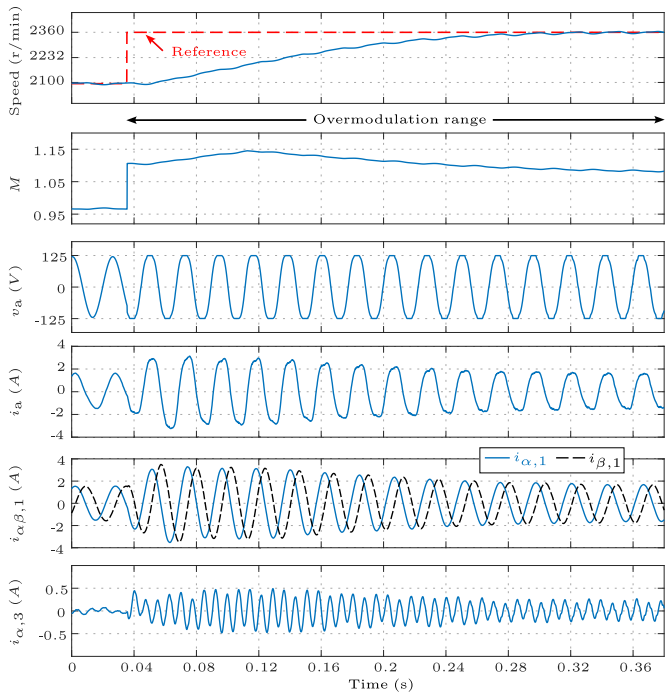

Fig. 17. Experimental speed transient with S6N1 and MCD$_\mu$. From top to bottom: rotor speed; reference M; inverter pole-voltage reference of phase a v_a; current of phase a i_a; $\alpha\beta_1$ current; and $\alpha\beta_3$ current.

C. Transient Experiments

In what follows, the behavior of the proposed methods during speed transients is analyzed. In particular, MCD$_\mu$ with the S6N1 machine is considered. A speed closed-loop scalar *V/f* control [39] is implemented to ensure that the motor follows the speed reference. The speed proportional-integral control gains are set according to [42]: 0.12-A/V proportional and 0.3-A/Vs integral gains, with 3.9-Hz bandwidth. The dc-link voltage is fixed at 250 V. Now, a resistive load is connected to the dc generator, coupled to the motor, to increase the torque load so that the six-phase stator current is 1.1 Arms at 2100 r/min, as depicted in Fig. 17 for time roughly until 0.04 s. Then, the speed reference is changed stepwise up to the rated speed 2360 r/min. To follow the speed reference, the speed closed-loop control increases the requested M from approximately 0.95 up to 1.15, thus entering the OVM range. To achieve such M, the inverter voltage references change smoothly and adopt a more square-like shape due to the $\alpha\beta_3$ harmonic injection. Although the $i_{\alpha\beta,3}$ current distorts the phase currents to some extent, the $i_{\alpha\beta,1}$ components remain close to sinusoidal. Consequently, besides greatly mitigating the current THD in steady state, the performance of MCD$_\mu$ during transients is satisfactory. In addition, it has been verified that the behavior of MCD$_{\alpha\beta\mu}$ is analogous to that of MCD$_\mu$, also proving to be suitable for transients.

VII. Conclusion

This article has proposed a generalized OVM strategy that is able to attain the minimum current THD, i.e., the MCD, for any n and NPs, and either SWA or AWA. Achieving the minimum current THD is highly desirable since the harmonic stator copper losses are proportional to the current THD. Two techniques are outlined: MCD$_\mu$ and MCD$_{\alpha\beta\mu}$. MCD$_\mu$ attains the minimum current THD while avoiding torque-producing harmonics. MCD$_{\alpha\beta\mu}$ also exploits such harmonics, with larger impedances, to further diminish the current THD and to reach the square waveform. These benefits gained by MCD$_{\alpha\beta\mu}$ come at the expense of some (small) increase in torque ripple. Both techniques have an offline and online part. In the former, for each modulation index, an offline optimization is performed to find the optimum amplitude and initial phase angle of the voltage harmonics to be injected. Then, these optimum values are stored in lookup tables used in the online part.

The benefits of these new methods over previous ones have been theoretically assessed for several kinds of multiphase motors. The theory is experimentally verified by using two six-phase induction motors, one with SWA and the other with AWA, when one and two NPs are set. Compared with previous techniques, the new MCDs achieve the smallest current THD in all scenarios. This is the first time that OVM with minimum current THD is attained for many multiphase machines.

Potential subjects of future work include devising an MCD OVM method suitable for closed-loop current controllers, particularly in scenarios where the injected harmonics could be altered by the control. Furthermore, the proposed solutions should be extended to other types of multiphase motors, such as synchronous ones, where closed-loop current control is practically mandatory and notable saliency may be present.

Appendix

For a given n with SWA [7], the magnitude-invariant vector space decomposition matrix is

$$\boldsymbol{T} = \frac{2}{n}\left[\boldsymbol{t}^{\cdot 0} \quad \boldsymbol{t}^{\cdot 1} \quad \cdots \quad \boldsymbol{t}^{\cdot \sigma} \quad \cdots \quad \boldsymbol{t}^{\cdot m}\right]^{\mathrm{T}} \tag{A.1}$$

where $\boldsymbol{t}^{\cdot\sigma}$ represents the element-wise power of vector $\boldsymbol{t}$ raised to the exponent σ (defined in Section II-A) where

$$\boldsymbol{t} = \left[\boldsymbol{\gamma^0} \quad \boldsymbol{\gamma^1} \quad \boldsymbol{\gamma^2} \quad \cdots \quad \boldsymbol{\gamma^{n-1}}\right] \tag{A.2}$$

with $\boldsymbol{\gamma} = \mathrm{e}^{\mathrm{j}2\pi/n}$. The transpose operation in (A.1) is carried out before replacing $\boldsymbol{t}^{\cdot\sigma}$. Moreover, the rows corresponding to $\sigma = 0$ for odd n or both $\sigma = 0$ and $\sigma = n/2$ for even n should be multiplied by $1/2$.

Analogously, for a given n with AWA [7], $\boldsymbol{T}$ can be expressed as in (A.1), but substituting instead the appropriate σ values for AWA and replacing (A.2) by

$$\boldsymbol{t} = \left[\boldsymbol{\gamma}^0\, \boldsymbol{\gamma}^1 \cdots \boldsymbol{\gamma}^{\frac{n}{l}-1} \middle| \boldsymbol{\gamma}^{\frac{2n}{l}} \boldsymbol{\gamma}^{\frac{2n}{l}+1} \cdots \boldsymbol{\gamma}^{\frac{2n}{l}+\frac{n}{l}-1} \middle| \cdots \right.$$
$$\left. \cdots \middle| \boldsymbol{\gamma}^{\frac{2n}{l}(l-1)} \boldsymbol{\gamma}^{\frac{2n}{l}(l-1)+1} \cdots \boldsymbol{\gamma}^{\frac{2n}{l}(l-1)+\frac{n}{l}-1} \right] \tag{A.3}$$

with $\boldsymbol{\gamma} = \mathrm{e}^{\mathrm{j}\pi/n}$. The vertical bars in (A.3) virtually divide $\boldsymbol{t}$ into l blocks, each containing n/l elements. Furthermore, the last row of (A.1) must be multiplied by $1/2$ for odd n.

$\boldsymbol{T}$ can be expressed as a real-valued matrix, denoted by $\bar{\boldsymbol{T}}$. It is obtained by separating the real and imaginary parts of each

row of $\boldsymbol{T}$ into two consecutive ones. Null rows are disregarded. Unlike $\boldsymbol{T}$, $\bar{\boldsymbol{T}}$ is square invertible.

REFERENCES

[1] E. Levi, R. Bojoi, F. Profumo, H. A. Toliyat, and S. Williamson, "Multiphase induction motor drives–A technology status review," *IET Electr. Power Appl.*, vol. 1, no. 4, pp. 489–516, Jul. 2007.

[2] E. Levi, "Multiphase electric machines for variable-speed applications," *IEEE Trans. Ind. Electron.*, vol. 55, no. 5, pp. 1893–1909, May 2008.

[3] A. G. Yepes, O. López, I. González-Prieto, M. J. Durán, and J. Doval-Gandoy, "A comprehensive survey on fault tolerance in multiphase ac drives, part 1: General overview considering multiple fault types," *Machines*, vol. 10, no. 3, Mar. 2022, Art. no. 208.

[4] A. Ghaderi, T. Umeno, and M. Sugai, "An altered PWM scheme for single-mode seamless control of ac traction motors for electric drive vehicles," *IEEE Trans. Ind. Electron.*, vol. 63, no. 3, pp. 1385–1394, Mar. 2016.

[5] C. Zhou, G. Yang, and J. Su, "PWM strategy with minimum harmonic distortion for dual three-phase permanent-magnet synchronous motor drives operating in the overmodulation region," *IEEE Trans. Power Electron.*, vol. 31, no. 2, pp. 1367–1380, Feb. 2016.

[6] A. G. Yepes and J. Doval-Gandoy, "Overmodulation method with adaptive x-y current limitation for five-phase induction motor drives," *IEEE Trans. Ind. Electron.*, vol. 69, no. 3, pp. 2240–2251, Mar. 2022.

[7] A. G. Yepes, J. Doval-Gandoy, and H. A. Toliyat, "Multifrequency current control for n-phase machines including antiwindup and distortion-free saturation with full DC-bus utilization," *IEEE Trans. Power Electron.*, vol. 34, no. 10, pp. 9891–9905, Oct. 2019.

[8] W. N. W. A. Munim, M. J. Duran, H. S. Che, M. Bermúdez, I. González-Prieto, and N. A. Rahim, "A unified analysis of the fault tolerance capability in six-phase induction motor drives," *IEEE Trans. Power Electron.*, vol. 32, no. 10, pp. 7824–7836, Oct. 2017.

[9] E. Levi, D. Dujic, M. Jones, and G. Grandi, "Analytical determination of dc-bus utilization limits in multiphase VSI supplied ac drives," *IEEE Trans. Energy Convers.*, vol. 23, no. 2, pp. 433–443, Jun. 2008.

[10] A. G. Yepes and J. Doval-Gandoy, "Simple carrier-based PWM for prolonged high DC-link utilization for symmetrical and asymmetrical n-phase AC drives," *IEEE Trans. Power Electron.*, vol. 36, no. 8, pp. 8696–8712, Aug. 2021.

[11] G. Carrasco and C. Silva, "Space vector PWM method for five-phase two-level VSI with minimum harmonic injection in the overmodulation region," *IEEE Trans. Ind. Electron.*, vol. 60, no. 5, pp. 2042–2053, May 2013.

[12] G. Yang et al., "Overmodulation strategy for seven-phase induction motors with optimum harmonic voltage injection based on sequential optimization scheme," *IEEE Trans. Power Electron.*, vol. 36, no. 12, pp. 14039–14050, Dec. 2021.

[13] J. Prieto, F. Barrero, M. J. Durán, S. Toral Marín, and M. A. Perales, "SVM procedure for n-phase VSI with low harmonic distortion in the overmodulation region," *IEEE Trans. Ind. Electron.*, vol. 61, no. 1, pp. 92–97, Jan. 2014.

[14] A. Iqbal and E. Levi, "Space vector modulation schemes for a five-phase voltage source inverter," in *Proc. Eur. Conf. Power Electron. Appl.*, 2005, pp. 1–12.

[15] T. Komrska, T. Glasberger, and Z. Peroutka, "Universal PWM modulator for multiphase drives with a minimum infinity-norm approach," *IEEE Trans. Ind. Electron.*, vol. 63, no. 10, pp. 5979–5987, Oct. 2016.

[16] M. Medina-Sánchez, A. G. Yepes, O. López, and J. Doval-Gandoy, "Assessment and exploitation of the minimum current harmonic distortion under overmodulation in five-phase induction motor drives," *IEEE Trans. Power Electron.*, vol. 38, no. 4, pp. 4289–4305, Apr. 2023.

[17] L. Vancini, M. Mengoni, G. Rizzoli, G. Sala, L. Zarri, and A. Tani, "Carrier-based PWM overmodulation strategies for five-phase inverters," *IEEE Trans. Power Electron.*, vol. 36, no. 6, pp. 6988–6999, Jun. 2021.

[18] M. J. Durán, J. Prieto, and F. Barrero, "Space vector PWM with reduced common-mode voltage for five-phase induction motor drives operating in overmodulation zone," *IEEE Trans. Power Electron.*, vol. 28, no. 8, pp. 4030–4040, Aug. 2013.

[19] F. Bu, T. Pu, Q. Liu, B. Ma, M. Degano, and C. Gerada, "Four-degree-of-freedom overmodulation strategy for five-phase space vector pulsewidth modulation," *IEEE J. Emerg. Sel. Topics Power Electron.*, vol. 9, no. 2, pp. 1578–1590, Apr. 2021.

[20] P. Stumpf, K. Bándy, and S. Halász, "Space vector based investigation of overmodulation region of inverter FED multiphase AC drives," in *Proc. IEEE 19th Int. Power Electron. Motion Control Conf.*, May 2021, pp. 506–513.

[21] M. Medina-Sánchez, A. G. Yepes, O. López, A. S. Abdel-Khalik, and J. Doval-Gandoy, "A carrier-based overmodulation strategy with minimum voltage distortion for symmetrical n-phase induction motor drives," *IEEE Trans. Power Electron.*, vol. 38, no. 12, pp. 15055–15071, Dec. 2023.

[22] G. Yang, S. Li, H. Hussain, Z. Bai, and J. Yang, "Establishing optimized harmonic injection order of sequential overmodulation strategies for seven-phase induction motors," *IEEE Trans. Energy Convers.*, vol. 38, no. 1, pp. 739–742, Mar. 2023.

[23] M. Medina-Sánchez, A. G. Yepes, O. López, A. S. Abdel-Khalik, and J. Doval-Gandoy, "A carrier-based overmodulation strategy with minimum voltage distortion for symmetrical nine-phase induction motor drives," in *Proc. Energy Convers. Congr. Expo.*, Dec. 2023, pp. 4712–4719.

[24] S. Paul and K. Basu, "A three-phase inverter based overmodulation strategy of asymmetrical six-phase induction machine," *IEEE Trans. Power Electron.*, vol. 36, no. 5, pp. 5802–5817, May 2021.

[25] S. Paul and K. Basu, "Overmodulation techniques of asymmetrical six-phase machine with optimum harmonic voltage injection," *IEEE Trans. Ind. Electron.*, vol. 68, no. 6, pp. 4679–4690, Jun. 2021.

[26] I. Zoric, M. Jones, and E. Levi, "Phase voltage harmonic imbalance in asymmetrical multiphase machines with single neutral point," in *Proc. IEEE 42nd Annu. Conf. Ind. Electron. Soc.*, Dec. 2016, pp. 4343–4348.

[27] J. Malvar et al., "Graphical diagram for subspace and sequence identification of harmonics in symmetrical multiphase machines," *IEEE Trans. Ind. Electron.*, vol. 61, no. 1, pp. 29–42, Jan. 2014.

[28] A. S. Abdel-Khalik, M. S. Abdel-Majeed, and S. Ahmed, "Effect of winding configuration on six-phase induction machine parameters and performance," *IEEE Access*, vol. 8, pp. 223009–223020, 2020.

[29] A. M. Shata, A. S. Abdel-Khalik, R. A. Hamdy, M. Z. Mostafa, and S. Ahmed, "Improved mathematical modeling of six phase induction machines based on fractional calculus," *IEEE Access*, vol. 9, pp. 53146–53155, 2021.

[30] J. Paredes, B. Prieto, M. Satrústegui, I. Elósegui, and P. González, "Improving the performance of a 1-MW induction machine by optimally shifting from a three-phase to a six-phase machine design by rearranging the coil connections," *IEEE Trans. Ind. Electron.*, vol. 68, no. 2, pp. 1035–1045, Feb. 2021.

[31] R. R. Bastos, T. S. de Souza, M. M. de Carvalho, L. A. R. Silva, and B. J. C. Filho, "Assessment of a nine-phase induction motor drive for metal industry applications," *IEEE Trans. Ind. Appl.*, vol. 56, no. 6, pp. 7217–7226, Nov./Dec. 2020.

[32] J. Pyrhönen, V. Hrabovcová, and S. Sudhoff, *Electrical Machine Drives Control: An Introduction*. Hoboken, NJ, USA: Wiley, 2016.

[33] IEEE Standard Test Procedure for Polyphase Induction Motors and Generators, IEEE Std. 112- 1991, 1991.

[34] A. S. Abdel-Khalik, A. Massoud, and S. Ahmed, "Standard three-phase stator frames for multiphase machines of prime-phase order: Optimal selection of slot/pole combination," *IEEE Access*, vol. 7, pp. 78239–78259, 2019.

[35] S. He et al., "Digital collaborative development of a high reliable auxiliary electric drive system for eTransportation: From dual three-phase PMSM to control algorithm," *IEEE Access*, vol. 8, pp. 178755–178769, 2020.

[36] X. Jiang, W. Huang, R. Cao, Z. Hao, and W. Jiang, "Electric drive system of dual-winding fault-tolerant permanent-magnet motor for aerospace applications," *IEEE Trans. Ind. Electron.*, vol. 62, no. 12, pp. 7322–7330, Dec. 2015.

[37] C.-C. Wang and C.-H. Fang, "Sensorless scalar-controlled induction motor drives with modified flux observer," *IEEE Trans. Energy Convers.*, vol. 18, no. 2, pp. 181–186, Jun. 2003.

[38] S. N. Vukosavic, L. S. Peric, and E. Levi, "Digital current controller with error-free feedback acquisition and active resistance," *IEEE Trans. Ind. Electron.*, vol. 65, no. 3, pp. 1980–1990, Mar. 2018.

[39] A. F. Abouzeid et al., "Control strategies for induction motors in railway traction applications," *Energies*, vol. 13, no. 3, Feb. 2020, Art. no. 700.

[40] A. S. Abdel-Khalik, R. A. Hamdy, A. M. Massoud, and S. Ahmed, "Post-fault control of scalar (V/F) controlled asymmetrical six-phase induction machines," *IEEE Access*, vol. 6, pp. 59211–59220, 2018.

[41] X. Zhang, T. Yang, and S. Bozhko, "Speed/torque ripple reduction of high-speed permanent magnet starters/generators with low inductance for more electric aircraft applications," *IEEE Trans. Transp. Electrif.*, vol. 8, no. 4, pp. 4431–4443, Dec. 2022.

[42] L. Harnefors, S. E. Saarakkala, and M. Hinkkanen, "Speed control of electrical drives using classical control methods," *IEEE Trans. Ind. Appl.*, vol. 49, no. 2, pp. 889–898, Mar./Apr. 2013.

Martín Medina-Sánchez (Graduate Student Member, IEEE) received the M.Sc. degree in automation and control engineering from the Escuela Superior Politécnica de Chimborazo, Riobamba, Ecuador, in 2017. He is currently working toward the Ph.D. degree in electrical engineering with the Applied Power Electronics Technology Research Group, Universidade de Vigo, Vigo, Spain.

His research interests include multiphase drives and power electronics.

Alejandro G. Yepes (Senior Member, IEEE) received the M.Sc. and Ph.D. degrees in electrical engineering from Universidade de Vigo, Vigo, Spain, in 2009 and 2011, respectively.

From 2016 to 2018, he was a Visiting Scholar with Texas A&M University, College Station, TX, USA. Since 2008, he has been with the Applied Power Electronics Technology Research Group, Universidade de Vigo. His research interests include the areas of ac power conversion.

Óscar López (Senior Member, IEEE) received the M.Sc. and Ph.D. degrees in electrical engineering from the University of Vigo, Vigo, Spain, in 2001 and 2009, respectively.

Since 2004, he has been an Assistant Professor with the University of Vigo. He is also a member of the Applied Power Electronics Technology Research Group, University of Vigo. His research interests include the areas of ac power switching converters technology.

Jesús Doval-Gandoy (Member, IEEE) received the M.Sc. degree in electrical engineering from the Polytechnic University of Madrid, Madrid, Spain, in 1991, and the Ph.D. degree in electrical engineering from Universidade de Vigo, Vigo, Spain, in 1999.

He is currently a Professor and the Head of the Applied Power Electronics Technology Research Group (APET), Universidade de Vigo. His research interests include the areas of ac power conversion.